American Journal of PHYSICAL ANTHROPOLOGY   WILEY

Relative tooth size, Bayesian inference, and *Homo naledi*

Joel D. Irish[1,2] | Mark Grabowski[1,3]

[1]Research Centre in Evolutionary Anthropology and Palaeoecology, School of Biological and Environmental Sciences, Liverpool John Moores University, Liverpool, UK

[2]The Centre for the Exploration of the Deep Human Journey, University of the Witwatersrand, Johannesburg, South Africa

[3]Centre for Ecology and Evolutionary Synthesis, Department of Biosciences, University of Oslo, Oslo, Norway

Correspondence
Joel D. Irish, Research Centre in Evolutionary Anthropology and Palaeoecology, School of Biological and Environmental Sciences, Liverpool John Moores University, Byrom Street, Liverpool, L3 3AF, UK.
Email: j.d.irish@ljmu.ac.uk

Abstract

Objectives: Size-corrected tooth crown measurements were used to estimate phenetic affinities among *Homo naledi* (∼335–236 ka) and 11 other Plio-Pleistocene and recent species. To assess further their efficacy, and identify dental evolutionary trends, the data were then quantitatively coded for phylogenetic analyses. Results from both methods contribute additional characterization of *H. naledi* relative to other hominins.

Materials and Methods: After division by their geometric mean, scaled mesiodistal and buccolingual dimensions were used in tooth size apportionment analysis to compare *H. naledi* with *Australopithecus africanus*, *A. afarensis*, *Paranthropus robustus*, *P. boisei*, *H. habilis*, *H. ergaster*, *H. erectus*, *H. heidelbergensis*, *H. neanderthalensis*, *H. sapiens*, and *Pan troglodytes*. These data produce equivalently scaled samples unaffected by interspecific size differences. The data were then gap-weighted for Bayesian inference.

Results: Congruence in interspecific relationships is evident between methods, and with many inferred from earlier systematic studies. However, the present results place *H. naledi* as a sister taxon to *H. habilis*, based on a symplesiomorphic pattern of relative tooth size. In the preferred Bayesian phylogram, *H. naledi* is nested within a clade comprising all *Homo* species, but it shares some characteristics with australopiths and, particularly, early *Homo*.

Discussion: Phylogenetic analyses of relative tooth size yield information about evolutionary dental trends not previously reported in *H. naledi* and the other hominins. Moreover, with an appropriate model these data recovered plausible evolutionary relationships. Together, the findings support recent study suggesting *H. naledi* originated long before the geological date of the Dinaledi Chamber, from which the specimens under study were recovered.

KEYWORDS
fossil hominins, gap-weighting, inhibitory cascade model, probabilistic phylogenetics, tooth size apportionment

1 | INTRODUCTION

In this study, relative tooth size of *Homo naledi* (Berger et al., 2015), ∼335–236 ka (Dirks et al., 2017) and other Plio-Pleistocene and recent hominin species are described and compared. It builds on prior work using tooth size apportionment (TSA) analysis to estimate phenetic affinities among several African species, including *Australopithecus sediba*, recent humans, and *Pan troglodytes* (Irish

et al., 2016). In TSA, the unit of study is the complete permanent dentition, rather than individual mesiodistal (MD) and buccolingual (BL) crown dimensions. These lengths and widths are first size corrected (below), to yield equivalently scaled samples, for submission to principal components analysis. Statistically, uncorrelated factor scores are used to place samples on axes of a scatterplot to visualize how crown size is differentially distributed, or apportioned, within the tooth rows. Because TSA is useful for comparing human individuals and groups (Harris, 1997, 1998; Harris & Bailit, 1988; Harris & Rathbun, 1991; Hemphill et al., 1992; Irish & Hemphill, 2001; Irish & Kenyhercz, 2013; Lukacs & Hemphill, 1993), which on an intraspecific level exhibit minimal variation, the technique was projected to be particularly effective when comparing more discernible interspecific differences of our hominin ancestors. This prediction was proven to be correct. The grouping of species (Irish et al., 2016) included in other, albeit, cladistic studies (Smith & Grine, 2008; Strait et al., 1997; Strait & Grine, 2004) is comparable, as are the affinities of A. sediba (Berger et al., 2010; Dembo et al., 2015, 2016; Irish et al., 2013, 2014).

As such, the initial intent here was to simply undertake an equivalent TSA analysis to dentally characterize H. naledi, estimate interspecific relationships, and assess its taxonomic classification. Earlier studies based on characters across the skeleton supported its inclusion in the genus Homo, but as a distinct member (Berger et al., 2015; Thackeray, 2015; Dembo et al., 2016; Irish et al., 2018; also see Holloway et al., 2018; Davies et al., 2020). A phenetic approach was deemed as most appropriate because continuous odontometric data do not lend themselves well to standard cladistic analyses; that is, they are typically reduced to a few ratios or crown areas qualitatively discretized into two or more states, along with other morphological characters (Berger et al., 2010; Strait & Grine, 2004). Of course, this same strategy applies to all continuous data with traditional phylogenetic analyses (Felsenstein, 2004; Parins-Fukuchi, 2018a, 2018b; Pimentcl & Riggins, 1987; Poe & Wiens, 2000; Pogue & Mickevich, 1990; Stevens, 1991; Thiele, 1993; Wiens, 1995), when they are not excluded entirely (Garcia-Cruz & Sosa, 2006; Poe & Wiens, 2000).

Yet, the benefits of continuous data, including more objective recording through standardized measurements, among others (below), encourage their use with phylogenetic inference. Recently, applicable models have been employed to analyze such data directly (e.g., Parins-Fukuchi, 2018a, 2018b; below), but a more established strategy is to apply one of several quantitative coding techniques. Some of these, to boost phylogenetic signal over qualitative discretizing, can return up to 30 states (Felsenstein, 2004; Garcia-Cruz & Sosa, 2006; Jones & Butler, 2018; Wiens, 2001). In reality, all morphological characters are "fundamentally quantitative," and in the present study they are treated as such (Wiens, 2001:689; Felsenstein, 2004; Schols et al., 2004), through the oft-used gap-weighted coding method (Garcia-Cruz & Sosa, 2006; Goloboff et al., 2006; Schols et al., 2004; Thiele, 1993).

Therefore, analyses of H. naledi, nine other African and Eurasian Plio-Pleistocene hominin species, two samples of recent African

H. sapiens, and Pan troglodytes proceed as follows. First, TSA analysis was used to estimate interspecific affinities with the continuous, scaled MD and BL dimensions. Second, given the demonstrated utility of this technique, it was decided to investigate further how these scaled data differ and distinguish among species. To do so, gap-weighted data were used in Bayesian inference under a Mkv (Lewis, 2001) or "standard discrete (morphology)" model (Huelsenbeck & Ronquist, 2001; Ronquist & Huelsenbeck, 2003; Ronquist et al., 2020:133). The results identify effects of presumed evolutionary trends on relative tooth size across species, beyond that previously reported. Moreover, with the appropriate parameters, these data can also recover plausible phylogenetic relationships. Finally, results from TSA and Bayesian analyses, in reference to prior studies, provide additional morphological characterization of H. naledi relative to the other species.

2 | MATERIALS AND METHODS

2.1 | The samples and their data sources

The H. naledi sample consists of 122 dental specimens from the Dinaledi Chamber of the Rising Star cave system, with mean MD and BL measurements in the present analyses from Berger et al. (2015). These fossils are directly linked to the ∼335–236 ka geological age (Dirks et al., 2017). Nine comparative Plio-Pleistocene samples were chosen based on two criteria. First, they provide a cross section of the three principal later hominin genera, though with an emphasis on Homo. Second, while analyses of individual hominins can be approximated using "meta-individuals" comprised of modern humans with complete dentitions (Irish et al., 2016:401), all samples have multiple MD and BL measurements for each tooth; this yields the most accurate means to reduce issues related to very small sample sizes. Thus, Kenyanthropus platyops, A. sediba, P. aethiopicus, H. rudolfensis, and H. floresiensis, among others with 0–1 observations for one or more teeth were not included. Mean data for six African samples are the same as in the prior TSA study (Irish et al., 2016). They are A. africanus (n = 307 total teeth), A. afarensis (n = 271), Paranthropus robustus (n = 377), P. boisei (n = 172), H. habilis (n = 93), and H. ergaster (n = 260). The H. habilis sample is small because it only comprises specimens from the species or, more broadly, the "1813 group" (Antón et al., 2014: 1236828–2), excluding H. rudolfensis or those of questioned attribution (e.g., KNM-ER 1482, 1590) (Antón et al., 2014; Joordens et al., 2013). Regarding H. ergaster (African H. erectus) few anterior teeth have been found in Africa, so MD and BL means again include data in 38 crowns from Dmanisi attributed to this species (Lordkipanidze et al., 2013; Martinón-Torres et al., 2008; Rightmire & Lordkipanidze, 2010). The non-African samples include H. erectus (n = 588) [data compiled for present study (SI Table S1) in Weidenreich, 1937, 1945; Wu & Chia, 1954; Jacob, 1973; Bermúdez de Castro, 1986; Wood, 1991; Wu & Poirier, 1995; Kaifu et al., 2005; Zaim et al., 2011; Xing et al., 2018], H. heidelbergensis (n = 789), and H. neanderthalensis (n = 821 teeth).

Mean MD and BL data for the latter two are from Berger et al. (2015), with information provided therein.

Representing *H. sapiens* are two samples of recent North (*n* = 20,674 teeth, 1412 individuals) and sub-Saharan Africans (*n* = 15,948, 822 inds.), recorded by the first author (Irish, 1993, 2000, 2005, 2006, 2008, 2010). Finally, to emphasize among-species taxonomic variation (Mahler, 1973) and illustrate the methodological efficacy of the phenetic analyses, while serving as the root in phylogenetic inference, the same *Pan troglodytes* data (*n* = 924 teeth, 70 individuals) used before are included (Irish et al., 2016).

2.2 | Odontometric measurements

For both *H. sapiens* samples, crown dimensions were recorded with needlepoint calipers accurate to 0.05 mm following Moorrees and Reed (1964). If antimeric pairs in an individual were present, mean MD and BL measurements were calculated; if only the right or left tooth remained, it was recorded, for up to 16 measurements in each isomere and 32 per dentition. For the other samples, measurements were reviewed for conformity to facilitate data compatibility, though inter-observer error obviously could not be tested.

Commonly in previous hominin studies, notably phylogenetic analyses, the genetic contribution of characters is often assumed but was not, or cannot, be estimated. This is an important point because if at least some characters lack a genetic basis, the results can be misleading (Wiens & Hillis, 1996). In modern humans narrow-sense heritability of MD and BL diameters was found to be high, in some cases $h^2 > 0.8$ (Alvesalo & Tigerstedt, 1974; Baydaş et al., 2005; Dempsey et al., 1995; Dempsey & Townsend, 2001; Hlusko et al., 2002; Kieser, 1990; Rizk et al., 2008; Townsend et al., 2003; Townsend & Brown, 1980). Recently, an association between body size and BL diameters was indicated (Hlusko et al., 2016), and a study of just MD diameters returned a lower h^2 of 0.51—though reproductive isolation and socioeconomic stress in the population sampled and small samples may have affected the value (per Stojanowski et al., 2017). Heritability of the scaled dental data has also not been assessed directly, but it should parallel the original MD and BL dimensions, given the correlation between datasets in the present study (*r* = 0.93, *p* = 0.00). At any rate, the h^2 value in Plio-Pleistocene hominins cannot be known. However, based on the above findings the prospect of relatively high heritability is, at a minimum, encouraging to estimate phenetic affinities and a phylogeny of characters from simple crown measurements readily available in the literature.

2.3 | TSA analysis

TSA analysis entails submitting a correlation matrix of data to principal components analysis (PCA), with the resulting uncorrelated components used to identify patterning of inter-tooth relationships. However, because this study is inter- rather than intraspecific in focus, the

methodology of previous TSA research (Harris, 1997, 1998; Harris & Bailit, 1988; Harris & Rathbun, 1991; Hemphill, 2016b; Hemphill et al., 1992; Irish & Hemphill, 2001; Lukacs & Hemphill, 1993) was tailored to address the substantial tooth size differences, for example, *Paranthropus* versus *Pan* (Irish et al., 2016). Like all skeletal measurements, odontometric data can be divided into: (1) (absolute) size and (2) shape (relative size) (Penrose, 1954; Rahman, 1962; Corruccini, 1973; Harris and Harris, 2007; Townsend et al., 2009; Irish et al., 2016). So a corrective technique in Jungers et al. (1995:145) they termed "DM_RAW," from Darroch and Mosimann (1985), was used to minimize size effects (also Collard & Wood, 2000) that dominate the first principal component, contra residual scores commonly used in modern human studies (Harris, 1997; Hemphill et al., 1992). The geometric mean (GM) is computed as the *n*th root of the product for all *n* dimensions (x) per case. Each dimension is divided by this mean (x/GM) for an average of 1.0 across the sample rows. Scaling "cancels out size differences by giving each [sample] the same average character state or magnitude over all the measurements taken on it" (Corruccini, 1973:747).

Data description was undertaken prior to submitting the correlation matrix of 32 DM_RAW-scaled mean MD and BL measurements to PCA. Group component scores were plotted in three dimensions to visualize phenetic variation using SPSS Ver. 26.0. Ideally, TSA analyses would be conducted with samples divided by sex, although this strategy was not followed in the aforementioned modern human comparisons. The reason is that, while sexual dimorphism may be a factor in absolute crown size differences between males and females in a common population (though see Harris, 2003), relative tooth size within the dentitions is unaffected (Harris & Rathbun, 1991; Hemphill, 2016b; Hemphill et al., 1992). Like heritability, the same cannot be claimed for Plio-Pleistocene species with significant differences in body size between the sexes. Regardless, it is out of necessity, including an inability to determine sex in most hominin specimens, considerable missing data, and a need to maximize sample sizes, that all specimens and individuals were pooled by species for analysis.

2.4 | Bayesian phylogenetic inference

Probabilistic or statistical methods to infer phylogenies, including Bayesian inference, are seeing increased use over nonprobabilistic methods like maximum parsimony. The reasons include methodological consistency, the ability to estimate branch lengths and evolutionary rates and, basically, better performance in genetic and morphological cases (Felsenstein, 2004; Lee et al., 2014; Wright and Hillis, 2014; EC.Europa.EU, 2016; Nascimento et al., 2017; Parins-Fukuchi, 2018a, 2018b; Guillerme & Brazeau, 2018). Indeed, the ".. . inconsistency of parsimony has been the strongest challenge to its use," although it works well with very large datasets to compare recently derived species (Felsenstein, 2004:121; EC.Europa. EU, 2016). The theories behind, overviews of, and techniques concerning Bayesian inference in parameter estimation are covered

thoroughly in the preceding references, and have been discussed in prior hominin studies (Dembo et al., 2016; Mongle et al., 2019). Additional, pertinent information is provided here in describing the analytical progression.

Phylogenies were inferred from quantitatively coded versions of DM_RAW-scaled data with, as noted, a Mkv model. These 32 scaled dimensions were gap-weighted using Thiele's (1993) method in MorphoCode 1.1 (Schols et al., 2004). It generates a data matrix, with the order and dispersal of means determined for each morphological character, and then converted to "ordered, multistate characters where the distance between means is represented by the distance between ordered character states" (Thiele, 1993; Wiens, 2001; Schols et al., 2004:2). This matrix of coded scaled data, in Nexus format, was submitted to MrBayes 3.2.7 (Huelsenbeck & Ronquist, 2001; Ronquist et al., 2020; Ronquist & Huelsenbeck, 2003) using the maximum number of states allowed by the program (see below).

Given the vast range of parameters, the aim was to begin simply, with a rooted strict-clock model and default, "so-called flat, uninformative, or vague [prior] distributions" (Felsenstein, 2004; EC.Europa. EU;, 2016; Ronquist et al., 2020:91). The latter are suggested to base the posterior distributions principally on the data—to establish their contribution (Ronquist et al., 2020; though see Felsenstein, 2004; Nascimento et al., 2017). From this, more complex parameters were added in a series of analyses. Of these, two relaxed-clock models representative of this progression are discussed: one basic and the other with many constraints, calibrations, and additional priors. All entail Bayesian molecular clock methods to estimate divergence among taxa (Hedges & Kumar, 2009; Nascimento et al., 2017).

Each model was analyzed using Markov chain Monte Carlo (MCMC) simulation with the Metropolis algorithm (EC.Europa. EU;, 2016; Felsenstein, 2004; Nascimento et al., 2017; Ronquist et al., 2020). Because the dataset is not large MrBayes default run values were used, with an increase in generations if needed. Two concurrent but independent analyses beginning with different random trees were run for 1,000,000 generations, with a sampling frequency of 500 to yield 2000 samples, and diagnostics calculated every 5000 generations. Runs consisted of one cold and three heated chains, with a 25% burn-in of samples from the cold chain so it could settle into its equilibrium distribution. This process allowed expedient calculation of convergence diagnostics to assess if a representative sample of trees resulted from the posterior probability distribution.

Established diagnostics used for the gap-weighted scaled data include: (1) standard deviation of split frequencies ≤0.01, (2) potential scale reduction factor (PSRF) of ~1.0 for all parameters, and (3) average effective sample sizes (ESS) of >200 (EC.Europa.EU, 2016; Felsenstein, 2004; Guillerme & Brazeau, 2018; Huelsenbeck & Ronquist, 2001; Nascimento et al., 2017; Ronquist et al., 2020; Ronquist & Huelsenbeck, 2003). If cut-offs were not met, the generation number was increased until minimums were achieved or exceeded, to yield similar trees from the independent runs. Finally, a cladogram with posterior probabilities, a.k.a. clade credibility values, and a phylogram with mean branch lengths were produced. Trees were rendered with FigTree 1.1.4. Related diagnostics include

posterior probabilities to determine final tree number, where ~1.0 specifies one tree (Ronquist et al., 2020).

The three clock analyses described here share several initial priors particular to the quantitatively coded data type [full parameter list in SI Table S2]. For state frequencies a symmetric dirichlet distribution fixed to infinity was used to correspond to the assumption of no transition rate asymmetry across sites (Ronquist et al., 2020). Coding bias was variable and type ordered, as necessary for the gap-weighted continuous data, where it is assumed evolution between states moves through intermediate states (0 < → 1 < → 2) (Felsenstein, 2004). MrBayes can handle 10 character states (0–9) if unordered, but only six if ordered (Ronquist et al., 2020). Therefore, states of 0–5 were calculated for each of the 32 scaled characters in Morphocode 1.1 for the input matrix.

First, for the strict-clock analysis (SI Table S2), a clock parameter was specified for branch lengths type, with a uniform prior and a fixed clock rate. Constant rates of evolution are assumed among taxa, where branch tips are presumed to be the same age (EC.Europa. EU, 2016; Felsenstein, 2004; Pybus, 2006; Ronquist et al., 2020). This approach is preferred for analyzing the same species with similar molecular evolution rates (Felsenstein, 2004), which cannot be assumed for the present hominin taxa.

Second, a basic relaxed-clock analysis (SI Table S2) was conducted. A model of this type is suggested for different species, because it can incorporate a prior distribution of evolutionary rates that vary among taxa and branches of a phylogeny (Felsenstein, 2004; Pybus, 2006). Like the strict-clock a relaxed-clock model is rooted, but information on root position is weaker. Therefore, following standard protocol a tree topology constraint was introduced to exclude *Pan* and force all other taxa into a monophyletic ingroup. The key change was to "'relax' the strict clock assumption" with an independent gamma rates (IGR) model of continuous uncorrelated variation across lineages (Ronquist et al., 2020:60). A related prior is a standard exponential rate of variance in effective branch lengths over time.

Third, a second relaxed-clock analysis (see SI Table S2) incorporated two important additions: (1) calibration node dating with a uniform prior of 6–8 Ma for the root, *Pan*, to designate the chimp/hominin split (Amster & Sella, 2016; Langergraber et al., 2012; Steiper & Seiffert, 2012), and (2) tip dating, where node depths are constrained by calibrating hominins with a fixed prior of maximum ages. The approach follows Dembo et al. (2016:20), with minor differences in first appearance dates (FAD) versus theirs based on "the oldest dates associated with the specimens." The FADs used are: *A. africanus* at 3.0 Ma (Herries et al., 2013); *A. afarensis*, 3.6 (Du et al., 2020; White et al., 2006); *P. robustus*, 2.0 (Herries and Adams, 2013; Gibbon et al., 2014); *P. boisei*, 2.3 (Wood & Lonergan, 2008); *H. habilis*, 2.4 (Spoor et al., 2015); *H. ergaster*, 1.9 (Du et al., 2018, 2020); *H. erectus*, 1.8 (Du et al., 2020; Wood & Lonergan, 2008); *H. heidelbergensis*, 0.6 (Wood & Lonergan, 2008); *H. neanderthalensis*, 0.2 (Devièse et al., 2017; Wood & Lonergan, 2008); *H. sapiens*, 0.315 (Richter et al., 2017). For *H. naledi* 0.335 ka (Dirks et al., 2017) was used, with the caveat that it applies to the Dinaledi chamber, and not necessarily the species' FAD.

Three other notable changes were made to this model. First, a gamma distribution was substituted for the rates prior (also used by Dembo et al., 2016), to accommodate rate variation across sites (EC. Europa.EU, 2016; Kuhner & Felsenstein, 1994; Ronquist et al., 2020). Second, the clock rate default prior, which measures node age as the number of expected substitutions per site, was swapped for a normal distribution to calibrate the tree in millions of years. A mean of 0.2 and a standard deviation of 0.02 designated that this distribution be truncated at 0, to yield positive values (Ronquist et al., 2020; Ronquist & Huelsenbeck, 2003). Third, a fossilized birth-death (FBD) prior with random sampling was substituted for the uniform branch lengths default (Ronquist et al., 2020). A standard birth-death prior (e.g., Dembo et al., 2016) is often used with dating and root constraints (Nascimento et al., 2017; Ronquist et al., 2020). However, the FBD is most appropriate for clock trees with calibrated external nodes (i.e., fossils) and if both extinct and extant species are included (Stadler, 2010; Heath et al., 2014; Heath, 2015; Stadler et al., 2018; Zhang et al., 2016; Ronquist et al., 2020). This prior describes the probability of tree and fossil data conditional on a number of birth-death parameters (SI Table S2), including speciation with branching (i.e., birth), extinction (death), and fossil preservation and recovery (sampling).

Finally, all clock models were compared by calculating Bayes factors ($B12$) from the marginal likelihoods that result when substituting the MCMC with the stepping-stone (ss) method (Xie et al., 2011). These factors represent the Bayesian equivalent of hypothesis testing to, in this case, select among the resulting topologies (Kass & Raftery, 1995). To calculate Bayes factors MCMC generation number was increased by a factor of 10 (Ronquist et al., 2020). The difference between logarithms of the marginal likelihoods was doubled [$2*\log e$ ($B12$)], where a product of 0–2 indicates "not worth more than a bare mention," 2–6 is "positive," 6–10 is "strong," and >10 is "very strong" evidence against or for model 1 (Mod_1) versus model 2 (Mod_2) (Kass & Raftery, 1993, 1995:777; Ronquist et al., 2020).

2.5 | Character independence

Before proceeding some mention of trait correlation is in order. In TSA analysis, statistical correlation of continuous data is negated with PCA, for example, $r \geq 0.5$ was returned in 23.5% of the 496 pairwise comparisons of MD and BL dimensions among the 13 samples. However, for phylogenetic analyses character independence is a critical assumption that, if violated, is expected to bias results (Billet & Bardin, 2019; Farris, 1983; Felsenstein, 2004; Gómez-Robles & Polly, 2012; Guillerme & Brazeau, 2018; Kay, 2015; Klingenberg, 2014; Kluge, 1989; O'Leary & Geisler, 1999; Strait & Grine, 2004). One potential source is character choice and coding (descriptively redundant, different parts of same feature described, etc.), although this too can be addressed (Strait & Grine, 2004: Guillerme & Brazeau, 2018). Most confounding is evolutionary correlation, said to predominantly affect morphological characters (though see Parins-Fukuchi, 2018a), whether coded qualitatively or quantitatively (Wiens, 2001). It may

relate to genetic linkage, similar selection pressures, pleiotropy, and structural and/or organismal integration (e.g., Adams & Felice, 2014; Felsenstein, 2004; Gómez-Robles & Polly, 2012; Guillerme & Brazeau, 2018; Hlusko & Mahaney, 2009; Klingenberg, 2014; Maddison, 2000; O'Leary & Geisler, 1999; Strait & Grine, 2004).

Evolutionary correlation can be investigated a posteriori through the phylogenetic hypotheses (Guillerme & Brazeau, 2018). Otherwise, with exception (below), effects on inference cannot be verified or addressed, especially with fossil taxa (Billet & Bardin, 2019; Felsenstein, 2004; Guillerme & Brazeau, 2018; O'Leary & Geisler, 1999). The same goes for possible homoplasy, another effect assumed inherent with morphological data—that nonetheless is a necessity when analyzing fossils (Kay, 2015; Wiens, 2001). A likely source of evolutionary correlation of particular relevance here is morphological integration (Billet & Bardin, 2019; Gómez-Robles & Polly, 2012; Klingenberg, 2014; Strait & Grine, 2004). It cannot be claimed that the DM-scaled dimensions of serially homologous teeth are an exception. Indeed, while incisors may be genetically independent from posterior teeth, at least in baboons (Hlusko & Mahaney, 2009), integration was found to affect crown shape in the postcanine dentition (Gómez-Robles & Polly, 2012); certain regions are affected more than others, including the mandibular dentition (relative to the maxillary), molars (vs. premolars), and UM3 and LP3. To address this lack of independence one suggested strategy is to merge dental observations into a few or one character, that is, "composite coding" (Billet & Bardin, 2019:268); however, doing so risks unverified a priori dismissal of phylogenetic signal (O'Leary & Geisler, 1999). And, given that the most substantial size variance occurs among tooth types (Harris, 2003), it would preclude exploring relative size variation among species in this study via phylogenetic inference.

Whatever the case, prospective issues with the present data are likely mitigated by Bayesian inference, said to be less affected by character correlation than parsimony, notably when comparing relatively few taxa (Guillerme & Brazeau, 2018). Also, this factor may not be as challenging for phylogenetic reconstruction as generally presumed (Adams & Felice, 2014; Parins-Fukuchi, 2018a). Evolutionary correlation is expected in closely related species, and vice versa (Felsenstein, 1985; Lajeunesse & Fox, 2015; Martins & Hansen, 1997). Simply put, the dilemma is that the question of correlation cannot be answered if the true phylogeny is not known, and the phylogeny cannot be reconstructed without knowing the answer (Felsenstein, 2002; P.D. Polly, personal communication, 2021). Therefore, like with any characters—qualitative or quantitative—a pragmatic approach (above) is to consider the plausibility, or the lack thereof, of the resulting phylogenies a posteriori.

3 | RESULTS

3.1 | Descriptive and TSA analyses

Mean MD and BL dimensions of *H. naledi* and the 12 other samples, with total number of teeth from which each were calculated, are

provided in Table 1. Maxillary and mandibular crown surface areas (MD x BL) were also determined and plotted (Figures 1 and 2). These are crude estimates of actual areas (Garn et al., 1977; Hemphill, 2016a), but can be useful indicators of absolute dental size variation among species (e.g., Evans et al., 2016; and below). For both isomeres, *H. naledi* is in the bottom half of the graphs among others of its assigned genus, about halfway between small-toothed *H. sapiens* and larger-toothed *H. habilis*. *Homo naledi* incisors and canines are comparable in crown area to those of *H. sapiens*, but the posterior teeth, especially P3, P4, M2, and M3 trend more toward other *Homo* species, except for *H. habilis* (compare individual measurements in Table 1).

The DM-scaled MD and BL dimensions are listed in Table 2. Compared with Table 1 the result of scaling is clear. For example, North African *H. sapiens* and *Pan* have the same UM1 MD diameter of 10.4 mm (Table 1), but the respective scaled values are 1.27 and 1.06 (Table 2). On the other hand, North African *H. sapiens* and *P. boisei* share a corrected LM1 MD value of 1.38 (Table 2), yet the absolute dimensions are 11.2 and 15.5 mm (Table 2). The effect of correction can be visualized by submitting the original and scaled data to UPGMA cluster analysis (Sokal & Sneath, 1963; SI Section S1). The former data yield two major size based clusters (SI Figure S1). The first comprises six 'large'-toothed species near the top of Figures 1 and 2 that, when summing all crown areas by sample, range between 1813 mm^2 for *H. ergaster* and 2483 total mm^2 for *P. boisei*. The second cluster, based on the UPGMA results and a "natural" break between Asian and African *H. erectus* (*ergaster*) evident in a bar graph of summed sample sizes (SI Figure S2), contains the seven "small"-toothed samples; the latter is at the bottom of Figures 1 and 2, with *Pan troglodytes* grouped among recent *Homo* taxa. Total crown areas range from 1154 for North African *H. sapiens* to 1638 mm^2 in *H. erectus* (SI Figure S2). In contrast, a dendrogram of DM-scaled values (SI Figure S3) more closely follows accepted phylogenies though, based on phenetic similarity, exceptions occur including: (1) a separate *Paranthropus* cluster, (2) *H. ergaster* and *H. erectus* in different clusters and, as pertinent to this study, (3) *H. naledi* and *H. habilis* linked together among other African species dated 3.6 to 1.9 Ma (discussed below).

For TSA analysis the correlation matrix of DM_RAW-scaled data was submitted to PCA. Un-rotated factor scores from the first three components with eigenvalues >1 were used to plot sample variation. Component loadings, eigenvalues, individual variance, and total variance explained, 90.7%, are listed in Table 3. The loadings are also presented as bar graphs (SI Figures S4–S6) to visualize those of the greatest importance in driving variation on axes of the scatterplot (Figure 3). By interpreting this output it can be determined how crown size is differentially apportioned or distributed along the maxillary and mandibular tooth rows, to compare variation in interspecific patterning.

As expected, the first component accounts for the most variation, 74.3%, which identifies the primary difference in relative intraspecific tooth size, and the longest branch in the subsequent

phylogenies (Polly et al., 2013; below). Like the first TSA hominin study (Irish et al., 2016), the *Paranthropus* pattern of megadont posterior and diminutive anterior teeth is evident. Except for the DM-scaled BL dimension of the UM1, 0.478, and scaled MD of the LP3, −0.217 (Table 3; SI Figure S4), strong loadings of 0.541–0.964 indicate relatively large cheek teeth in both isomeres; this influence pushed *P. boisei* and *P. robustus* toward the positive end of the PC1-axis (Figure 3). The first exception, the DM-scaled UM1 BL dimension with a lower loading of 0.541 for the scaled MD, marks the extreme M1 < M2 < M3 size progression in this genus. The second exception, the negative loading for DM-scaled LP3 MD, is more a function of the sectorial premolar in *Pan* near the opposite end of the axis. Otherwise, the latter species' location is driven by loadings of −0.786 to −0.978 for relatively large I1, I2, and C in both maxilla and mandible. The remaining samples plot between these two extremes. The stimulus for this distribution is apparent in Table 2, where except for UM1 and LM1, the *Paranthropus* taxa have the largest size-corrected posterior diameters, especially compared to *Pan*. The opposite holds for anterior teeth; *Pan* has the largest scaled diameters, and *P. boisei* and *P. robustus* the smallest.

The second component accounts for 11.6% of the variance, with samples separated by differences in the molar class. As implied on component 1, the maxillary and mandibular first molars are responsible. In Table 3 (and SI Figure S5), DM-scaled MD and BL values for the UM1 are strongly negative, −0.645 and − 0.854. Loadings for the LM1 are moderately (−0.0480) and strongly (−0.656) negative. Thus, M1s in both isomeres of the lowest scoring samples on the PC2-axis are large relative to the M2s and M3s, to explain why most *Homo* species group at the farthest, negative end (Figure 3). In particular, *H. sapiens* exhibits the typical M1 > M2 > M3 gradient, evidenced by size-corrected MD and BL dimensions for UM1 and LM1 (Table 2); this stands in contrast to the australopith samples near the positive end of the PC2-axis. This patterning likely reflects size effects of the inhibitory cascade model discerned in hominins (Evans et al., 2016; and below); yet, a closer inspection of the loadings also suggests shape differences, where samples toward the positive end of the axis have larger scaled MD than BL diameters for M2s and M3s, unlike those at the negative end. A more obvious factor is the loading 0.846 for the DM-scaled MD of the LP3 (above); it drives *Pan* toward the positive end, and affects *H. naledi*, with the latter's slightly greater DM-scaled MD (0.99) dimension than BL (0.96) (Table 2). Again, values are relative to those of the full dentition, as seen by less variation in the actual MD (9.0 mm) and BL (8.8 mm) LP3 dimensions in *H. naledi* (Table 1). Though sample size must be considered, also note the identical MD and BL dimensions for this tooth (10 mm) in *H. habilis* contra all remaining *Homo* species.

Finally, component 3 accounts for only 4.9% of the variation. There are no strong loadings, though several are moderate (|0.3–0.4|) (Table 3; SI Figure S6). Low scoring samples on the PC3-axis, such as *H. naledi* and *H. habilis*, are there in part because of: (1) larger DM-scaled MD (−0.304) relative to BL dimensions for the UI1, (2) larger

TABLE 1 Mean maxillary and mandibular mesiodistal (MD) and buccolingual (BL) diameters for the 13 samples.

	PAN		PBO		PRO		AFA		AFR		HNA		HHA		HEG		HER		HHE		HNE		HSS		HSN	
	MD	BL	MD	BL	MD	BL	MD	BL	MD	BL	MD	BL	MD	BL	MD	BL	MD	BL	MD	BL	MD	BL	MD	BL	MD	BL
UI1	11.7 (64)[a]	9.4 (64)	9.2 (5)	7.0 (5)	8.8 (17)	7.2 (17)	10.7 (7)	8.4 (8)	10.5 (8)	8.4 (8)	9.4 (3)	6.5 (5)	10.8 (4)	7.5 (4)	11.4 (3)	7.8 (3)	10.2 (10)	8.2 (11)	9.6 (21)	7.8 (23)	9.7 (28)	8.5 (37)	8.6 (358)	7.0 (412)	8.6 (357)	7.0 (459)
UI2	8.6 (44)	8.6 (44)	7.9 (5)	6.6 (5)	6.7 (12)	6.8 (12)	7.5 (9)	7.2 (9)	6.8 (10)	6.9 (10)	6.6 (4)	6.2 (8)	7.2 (6)	6.8 (6)	8.1 (5)	7.6 (5)	7.5 (3)	8.1 (3)	7.7 (19)	7.8 (21)	8.0 (35)	8.4 (41)	6.8 (388)	6.3 (430)	6.7 (417)	6.3 (503)
UC	11.1 (60)	12.5 (60)	8.6 (5)	8.8 (5)	8.4 (26)	9.2 (26)	9.9 (15)	10.8 (15)	10.0 (13)	10.3 (13)	8.1 (10)	8.6 (9)	9.5 (6)	9.9 (6)	9.8 (6)	9.8 (6)	9.4 (8)	10.2 (8)	8.8 (27)	9.8 (29)	8.8 (28)	10.1 (29)	7.5 (554)	8.2 (575)	7.4 (600)	8.1 (668)
UP3	8.0 (70)	10.3 (70)	10.5 (9)	14.4 (9)	9.7 (28)	13.9 (28)	8.8 (12)	12.4 (10)	9.2 (22)	12.8 (22)	8.0 (10)	10.5 (10)	9.1 (9)	12.0 (9)	8.8 (10)	12.5 (10)	8.3 (27)	11.6 (27)	7.9 (25)	10.6 (25)	8.0 (16)	10.6 (17)	7.0 (653)	9.3 (688)	6.9 (685)	8.9 (770)
UP4	7.2 (49)	10.1 (49)	11.6 (4)	16.3 (4)	10.4 (31)	15.0 (31)	9.1 (18)	12.4 (12)	9.3 (14)	13.5 (14)	8.1 (7)	11.0 (7)	9.2 (9)	12.0 (9)	8.5 (7)	11.9 (7)	7.9 (37)	11.4 (36)	7.6 (22)	10.3 (23)	7.8 (21)	10.6 (19)	6.7 (631)	9.2 (658)	6.6 (655)	9.1 (804)
UM1	10.4 (70)	11.4 (70)	14.1 (13)	15.0 (13)	13.1 (34)	14.1 (34)	12.0 (16)	13.4 (13)	12.9 (19)	13.9 (19)	11.6 (12)	11.7 (13)	12.9 (13)	13.0 (13)	12.8 (12)	13.3 (11)	11.6 (33)	13.0 (32)	11.2 (25)	11.9 (24)	11.6 (23)	12.3 (24)	10.4 (609)	11.2 (718)	10.4 (625)	11.2 (914)
UM2	10.3 (50)	11.6 (50)	15.5 (8)	16.8 (8)	14.1 (26)	15.7 (26)	12.9 (10)	14.6 (11)	14.0 (20)	15.7 (20)	12.2 (11)	12.8 (9)	13.1 (10)	14.6 (10)	12.7 (8)	13.4 (8)	11.3 (25)	13.1 (25)	10.2 (24)	12.3 (23)	10.9 (28)	12.5 (28)	9.8 (659)	11.3 (714)	9.6 (845)	11.1 (951)
UM3	9.6 (57)	11.0 (57)	14.1 (5)	17.4 (5)	14.7 (30)	16.4 (30)	12.7 (11)	14.5 (11)	14.0 (14)	15.9 (24)	11.6 (7)	12.4 (7)	12.6 (8)	14.6 (8)	12.4 (5)	14.0 (5)	9.7 (11)	12.2 (11)	8.9 (26)	11.6 (27)	9.9 (22)	12.3 (21)	8.8 (427)	11.0 (458)	8.9 (717)	10.7 (737)

	PAN		PBO		PRO		AFA		AFR		HNA		HHA		HEG		HER		HHE		HNE		HSS		HSN	
	MD	BL	MD	BL	MD	BL	MD	BL	MD	BL	MD	BL	MD	BL	MD	BL	MD	BL	MD	BL	MD	BL	MD	BL	MD	BL
LI1	7.8 (62)	8.7 (62)	5.3 (9)	6.7 (9)	5.4 (10)	6.1 (10)	6.7 (7)	7.1 (8)	6.1 (9)	6.5 (9)	6.1 (7)	5.4 (7)	6.5 (2)	6.9 (2)	5.7 (4)	6.5 (4)	6.6 (6)	6.4 (6)	5.6 (21)	6.7 (22)	5.6 (9)	7.2 (16)	5.2 (335)	5.7 (349)	5.3 (325)	5.8 (439)
LI2	8.4 (42)	9.1 (42)	5.8 (4)	7.2 (4)	6.5 (7)	6.6 (7)	6.7 (7)	8.0 (6)	7.2 (10)	7.8 (10)	6.9 (5)	5.9 (6)	7.7 (2)	7.5 (2)	7.2 (8)	7.2 (8)	7.0 (9)	7.1 (10)	6.5 (19)	7.3 (20)	6.8 (23)	7.8 (31)	5.8 (383)	6.1 (403)	5.8 (436)	6.1 (536)
LC	10.6 (61)	12.3 (61)	7.9 (11)	9.0 (11)	7.7 (20)	8.2 (20)	8.8 (13)	10.4 (16)	9.3 (23)	10.1 (23)	7.1 (7)	7.1 (7)	9.0 (3)	9.2 (3)	9.2 (6)	8.9 (6)	8.2 (10)	9.1 (12)	7.6 (23)	8.7 (24)	7.8 (36)	8.8 (41)	6.9 (449)	7.3 (475)	6.6 (497)	7.4 (618)
LP3	10.4 (69)	8.3 (69)	10.4 (10)	13.5 (10)	9.9 (24)	12.1 (24)	9.6 (27)	10.6 (26)	9.6 (18)	11.4 (18)	9.0 (9)	8.8 (10)	10.0 (3)	10.0 (3)	9.5 (11)	10.2 (12)	8.7 (21)	9.9 (20)	7.9 (22)	8.9 (22)	7.9 (20)	9.1 (21)	7.1 (499)	7.9 (517)	6.8 (634)	7.7 (725)
LP4	7.9 (48)	8.6 (48)	12.9 (19)	13.3 (18)	11.0 (22)	12.8 (22)	9.8 (24)	11.0 (21)	10.2 (24)	11.6 (24)	8.7 (6)	9.1 (6)	10.5 (3)	10.9 (3)	8.8 (9)	9.9 (9)	8.6 (16)	10.1 (17)	7.2 (26)	8.7 (26)	7.8 (23)	9.4 (25)	7.2 (469)	8.2 (510)	7.0 (616)	8.0 (751)
LM1	10.9 (70)	9.7 (70)	15.5 (19)	14.0 (19)	14.5 (33)	14.0 (19)	13.1 (32)	12.6 (26)	14.0 (27)	13.0 (27)	12.2 (11)	10.7 (11)	13.8 (5)	11.8 (5)	13.0 (16)	11.7 (16)	12.5 (30)	11.9 (30)	11.3 (29)	10.6 (29)	11.8 (38)	11.1 (40)	11.4 (443)	10.4 (533)	11.2 (501)	10.4 (841)
LM2	11.3 (50)	10.5 (50)	17.5 (20)	15.9 (20)	16.0 (26)	14.8 (26)	14.3 (31)	13.4 (27)	15.7 (35)	14.5 (35)	13.3 (9)	11.2 (9)	15.0 (5)	13.4 (5)	13.6 (16)	12.1 (16)	13.2 (29)	12.6 (28)	11.2 (29)	10.5 (29)	12.1 (26)	11.3 (27)	10.7 (462)	10.2 (547)	10.7 (728)	10.0 (919)
LM3	10.7 (58)	10.2 (58)	18.0 (26)	15.4 (26)	16.8 (31)	14.5 (31)	15.3 (26)	13.5 (23)	16.3 (31)	14.6 (31)	13.4 (6)	12.1 (5)	15.3 (5)	13.0 (5)	13.9 (10)	12.2 (11)	12.2 (19)	11.4 (19)	11.5 (32)	10.0 (32)	12.0 (18)	11.0 (20)	10.6 (319)	10.0 (343)	10.6 (679)	9.9 (722)

Note: Odontometric data from published and directly-recorded measurements (see text for details).

Abbreviations: AFA, *A. afarensis*; AFR, *A. africanus*; HNA, *H. naledi*; HHA, *H. habilis*; HEG, *H. ergaster*; HER, *H. erectus*; HHE, *H. heidelbergensis*, HNE, *H. neanderthalensis*; HSS, *H. sapiens* (SsA); HSN, *H. sapiens* (NAf) (see text for details); PAN, pan troglodytes; PBO, *P. boisei*; PRO, *P. robustus*.

[a]Values in parentheses identify the number of teeth measured to calculate mean MD and BL diameters.

FIGURE 1 Line plot showing tooth-by-tooth trends in absolute occlusal surface areas of the maxillary dentition in mm² by sample. Line colors and format apply loosely to genus (e.g., Figures 3, 6, SI Figure S2), but are primarily used to differentiate samples. See text for sample compositions
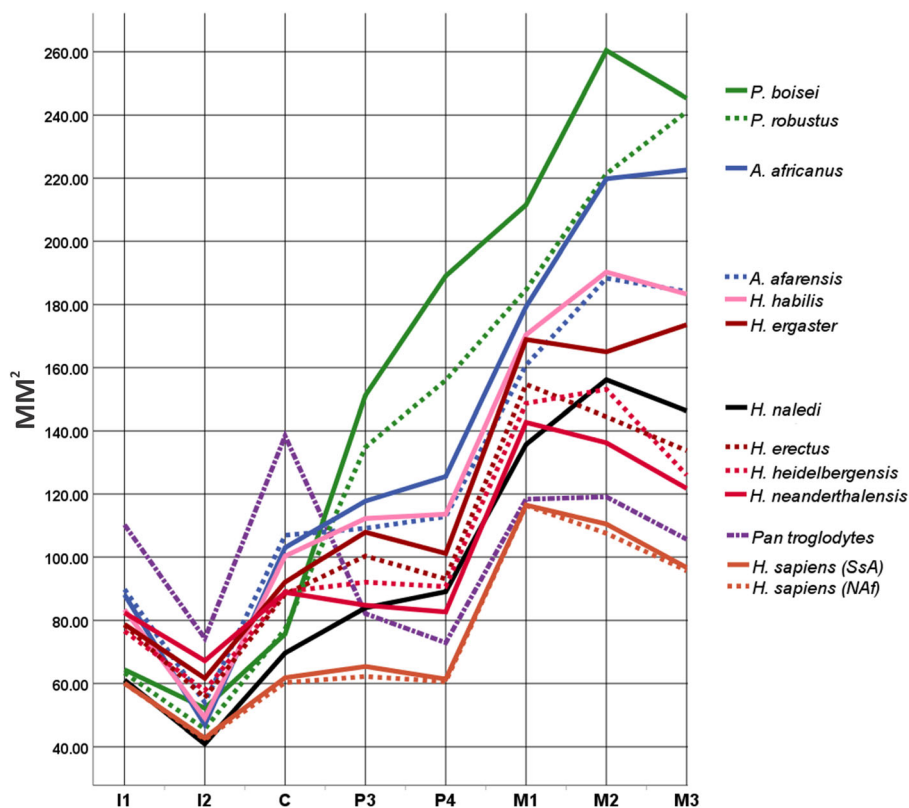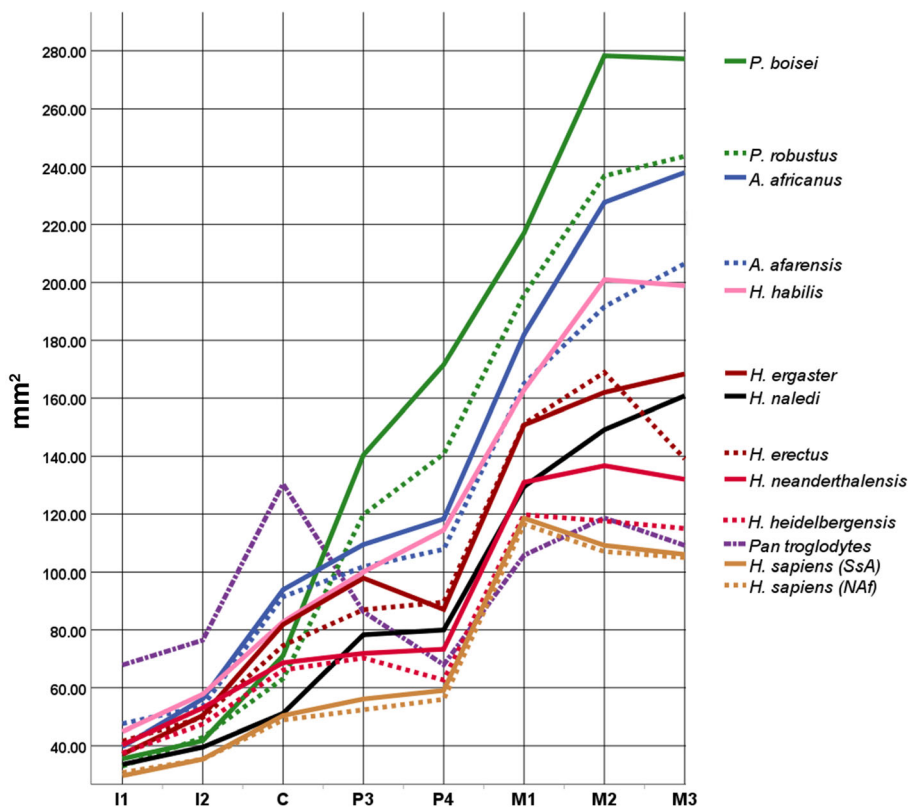

FIGURE 2 Line plot showing tooth-by-tooth trends in absolute occlusal surface areas of the mandibular dentition in mm² by sample. Line colors and format apply loosely to genus (e.g., Figures 3, 6, SI Figure S2), but are primarily used to differentiate samples. See text for sample compositions

DM-scaled MD (−0.402) relative to BL for the UM1, and (3) larger DM-scaled MD (−0.390) relative to BL for LI2 than other species. These teeth may be characterized as relatively long and narrow. Near the top of the axis samples have a contrary pattern, while the DM-scaled MD dimension of the LM1 (−0.310) and BL dimension of LP3 (0.390) are also involved (see Table 2).

TABLE 2 DM_Raw size-corrected mesiodistal (MD) and buccolingual (BL) diameters for the samples used in the TSA analyses

	PAN		PBO		PRO		AFA		AFR		HNA		HHA		HEG		HER		HHE		HNE		HSS		HSN	
	MD	BL	MD	BL	MD	BL	MD	BL	MD	BL	MD	BL	MD	BL	MD	BL	MD	BL	MD	BL	MD	BL	MD	BL	MD	BL
UI1	1.20	0.96	0.82	0.62	0.83	0.68	1.01	0.79	0.96	0.77	1.03	0.71	1.05	0.71	1.12	0.77	1.05	0.84	1.02	0.83	1.03	0.90	1.04	0.85	1.05	0.86
UI2	0.88	0.88	0.70	0.59	0.63	0.64	0.71	0.68	0.62	0.63	0.72	0.69	0.68	0.64	0.80	0.75	0.77	0.83	0.80	0.80	0.85	0.89	0.83	0.77	0.82	0.78
UC	1.13	1.27	0.77	0.78	0.79	0.86	0.94	1.02	0.92	0.95	0.89	0.94	0.92	0.97	0.96	0.96	0.96	1.05	0.95	1.04	0.93	1.07	0.92	1.00	0.92	0.99
UP3	0.82	1.05	0.93	1.28	0.91	1.30	0.83	1.17	0.85	1.18	0.88	1.15	0.87	1.15	0.87	1.23	0.85	1.19	0.87	1.17	0.85	1.13	0.86	1.13	0.85	1.10
UP4	0.73	1.03	1.03	1.45	0.98	1.41	0.86	1.17	0.85	1.24	0.89	1.21	0.88	1.15	0.84	1.17	0.81	1.17	0.85	1.18	0.83	1.13	0.81	1.12	0.82	1.12
UM1	1.06	1.16	1.25	1.33	1.23	1.32	1.13	1.27	1.19	1.28	1.27	1.28	1.23	1.24	1.26	1.31	1.19	1.33	1.24	1.33	1.23	1.31	1.27	1.36	1.27	1.38
UM2	1.04	1.18	1.38	1.50	1.32	1.47	1.22	1.38	1.29	1.44	1.34	1.40	1.23	1.37	1.25	1.32	1.16	1.34	1.22	1.39	1.16	1.33	1.20	1.37	1.19	1.36
UM3	0.98	1.13	1.25	1.55	1.38	1.54	1.20	1.37	1.29	1.46	1.27	1.36	1.19	1.37	1.22	1.38	0.99	1.25	1.05	1.33	1.05	1.31	1.07	1.34	1.10	1.31
LI1	0.79	0.89	0.47	0.60	0.51	0.57	0.63	0.67	0.56	0.60	0.67	0.59	0.61	0.65	0.56	0.64	0.68	0.66	0.62	0.70	0.59	0.76	0.64	0.69	0.65	0.71
LI2	0.85	0.93	0.51	0.64	0.61	0.62	0.63	0.76	0.66	0.72	0.76	0.65	0.72	0.70	0.71	0.71	0.72	0.73	0.70	0.76	0.71	0.83	0.70	0.74	0.71	0.75
LC	1.08	1.25	0.70	0.80	0.72	0.77	0.83	0.98	0.85	0.93	0.78	0.78	0.85	0.87	0.91	0.88	0.84	0.93	0.82	0.92	0.83	0.93	0.84	0.89	0.81	0.90
LP3	1.06	0.84	0.93	1.20	0.93	1.13	0.91	1.00	0.89	1.05	0.99	0.96	0.93	1.02	0.95	1.00	0.89	1.02	0.91	1.00	0.84	0.97	0.86	0.96	0.84	0.94
LP4	0.80	0.88	1.15	1.18	1.03	1.20	0.93	1.04	0.94	1.06	0.95	1.00	0.99	1.06	0.87	0.97	0.88	1.04	0.83	0.99	0.83	1.00	0.87	1.00	0.86	0.99
LM1	1.11	0.99	1.38	1.25	1.36	1.27	1.24	1.19	1.29	1.19	1.34	1.17	1.32	1.17	1.28	1.15	1.28	1.22	1.28	1.19	1.25	1.18	1.38	1.27	1.38	1.27
LM2	1.16	1.07	1.56	1.41	1.50	1.39	1.35	1.27	1.44	1.33	1.46	1.23	1.48	1.30	1.34	1.19	1.35	1.29	1.31	1.23	1.28	1.20	1.30	1.24	1.32	1.23
LM3	1.09	1.04	1.60	1.37	1.58	1.36	1.45	1.28	1.50	1.34	1.47	1.33	1.47	1.25	1.37	1.20	1.25	1.17	1.28	1.14	1.27	1.17	1.28	1.21	1.31	1.21

Note: DM_Raw size-correction–see main text for details.

Abbreviations: AFA, *A. afarensis*; AFR, *A. africanus*; HHA, *H. habilis*; HEG, *H. ergaster*; HER, *H. erectus*; HHE, *H. heidelbergensis*; HNA, *H. naledi*; HNE, *H. neanderthalensis*; HSN, *H. sapiens* (NAf); HSS, *H. sapiens* (SsA); PAN, *Pan troglodytes*; PBO, *P. boisei*; PRO, *P. robustus* (see text for details).

3.2 | Bayesian phylogenetic inference

The strict-clock cladogram (SI Figure S7) is nearly identical to the abovementioned UPGMA dendrogram (SI Figure S3). This is unsurprising, given the model (as above) assumes constant evolution rates and age among taxa, to yield phylogenies based largely on overall similarity. Again, the *Paranthropus* sister taxa are an outgroup to two larger hominin clades. The first contains African-only species, but with a polytomous node for daughter taxa *A. afarensis*, *A. africanus*, *H. ergaster* and *H. naledi/H. habilis*—which are again sister taxa. The second large clade comprises the five recent *Homo* samples. As before, *H. ergaster* and *H. erectus* are separated, in conflict with conventional interpretations of a single lineage. These three main clades also match groupings in the Figure 3 ordination. Clade credibility values, 52.3–100%, indicate the proportion of trees in the MCMC sample having these clades. The lowest is for the node between *H. erectus* and sister taxa *H. heidelbergensis* and *H. neanderthalensis*. The highest identifies four nodes: (1) *Pan* and the rest, (2) both *Paranthropus* species, (3) the latter and all others, and (4) both *H. sapiens* samples. The remaining values, 55.7–97.8%, include 75.4% for *H. habilis/H. naledi*. Posterior probabilities diagnostics indicate, among others (SI Table S3), a final tree number of 1.0, to provide support for a single tree, and a marginal likelihood of −617.48.

An MCMC run of 2,000,000 generations was necessary for the basic relaxed-clock analysis to achieve a standard deviation of split frequencies <0.01 (SI Table S3); this value indicates that similar trees from each run and a representative sample from the posterior probability were obtained. The marginal likelihood of −606.66, subtracted from that of the strict-clock and doubled [$2*\log_e(B12)$] yielded a product of 21.64, meaning that, based on Bayes factor comparisons, this model is strongly favored over the first. In line with accepted phylogenetic hypotheses, the *Paranthropus* sister taxa now form a clade with *A. africanus*, within the large hominin clade of African-only species as above (SI Figure S8). Clade credibility values are higher, 64.4–100%. The lowest identifies the node between *H. sapiens* and the other more recent *Homo* species. It is 75.9% for sister taxa *H. habilis* and *H. naledi*, 87.4% between the early *Homo* and four australopiths from the African-only clade, and 87.9% for *H. heidelbergensis/H. neanderthalensis*. The rest are ~100%. Nevertheless, the maximum a posteriori tree is unresolved with two polytomies, one at the base of the five recent *Homo* samples, and the second linking *A. afarensis*, *H. ergaster*, and *H. naledi/H. habilis* sister taxa.

Finally, the dated relaxed-clock analysis using the fossilized birth-death (FBD) branch lengths and gamma rates priors produced the fully resolved phylogram in Figure 4 (SI Table S3), after a run of 3,000,000 generations. Rate variation is demonstrated by branch lengths relative to the first appearance dates. *Australopithecus afarensis* is an outgroup to the other hominins, and all *Homo* species form a clade separate from the australopiths with a 69.4% credibility value. Other values include 74.2% between *H. ergaster* and *H. erectus*, in line with conventional views of a single lineage, and 88.1–100% for the seven remaining nodes, with *H. habilis/H. naledi* at 90.1%. Posterior probabilities diagnostics again indicate a single tree, and the marginal

TABLE 3 Loadings, eigenvalues, and the variance explained for the first three principal components based on size corrected maxillary and mandibular measurements in the 13 samples

Variable	Component		
	1	2	3
DM_MDUI1	**−0.918**	−0.027	−0.304
DM_MDUI2	**−0.786**	−0.441	0.098
DM_MDUC	**−0.963**	0.175	−0.002
DM_MDUP3	**0.832**	−0.035	0.133
DM_MDUP4	**0.934**	0.139	0.164
DM_MDUM1	**0.541**	**−0.645**	−0.402
DM_MDUM2	**0.934**	0.190	−0.240
DM_MDUM3	**0.815**	0.385	−0.251
DM_BLUI1	**−0.923**	−0.282	0.156
DM_BLUI2	**−0.845**	−0.390	0.193
DM_BLUC	**−0.978**	0.061	0.129
DM_BLUP3	**0.843**	0.073	0.295
DM_BLUP4	**0.922**	0.157	0.276
DM_BLUM1	0.478	**−0.854**	0.015
DM_BLUM2	**0.958**	−0.089	0.000
DM_BLUM3	**0.964**	0.082	0.034
DM_MDLI1	**−0.871**	0.129	−0.245
DM_MDLI21	**−0.873**	0.086	−0.390
DM_MDLC	**−0.885**	0.345	−0.030
DM_MDLP3	−0.217	**0.846**	−0.178
DM_MDLP4	**0.877**	0.342	0.031
DM_MDLM1	**0.767**	−0.480	−0.310
DM_MDLM2	**0.954**	0.197	−0.130
DM_MDLM3	**0.948**	0.235	−0.086
DM_BLLI1	**−0.909**	−0.031	0.257
DM_BLLI2	**−0.928**	0.013	0.283
DM_BLLC	**−0.873**	0.290	0.308
DM_BLLP3	**0.902**	0.007	0.390
DM_BLLP4	**0.930**	0.084	0.282
DM_BLLM1	**0.684**	**−0.656**	0.032
DM_BLLM2	**0.929**	0.030	0.168
DM_BLLM3	**0.929**	0.152	−0.172
Eigenvalue	23.766	3.702	1.569
Variance (%)	74.268	11.569	4.905
Total Variance	74.268	85.837	90.742

Note: Values in bold-face indicate strong loadings, that is, ≥|0.5| (see text for details).

likelihood is −600.94. With Bayes factor criteria for 'very strong' evidence a product of >10 (Kass & Raftery, 1995; Ronquist et al., 2020), those between this model and the other two (Mod₁ and Mod₂) are, respectively, 33.08 and 11.44. This dated relaxed-clock model is deemed the best in terms of the tree topology, in that it provides the most likely a posteriori hypothesis (Kass & Raftery, 1995).
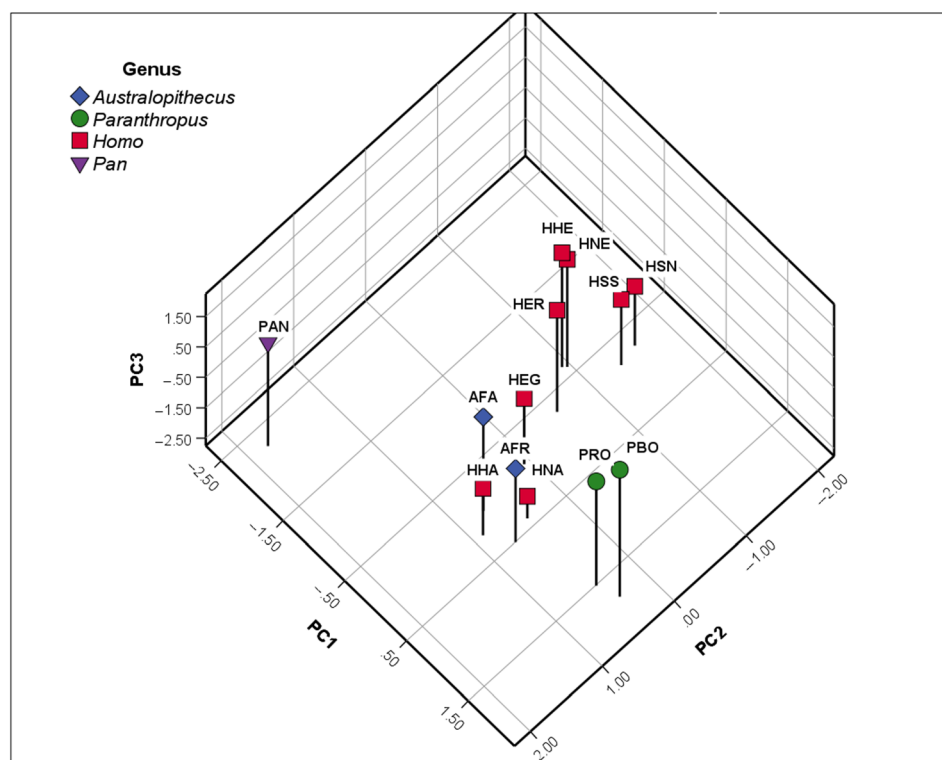
FIGURE 3 Three-dimensional ordination of retained principal component scores for tooth size apportionment (TSA) in the dentition of *H. naledi* (HNA) and 12 comparative samples. Accounts for 90.7% of the total variance (74.2% on PC1, 11.6% on PC2, and 4.9% on PC3). AFA, *A. afarensis*; AFR, *A. africanus*; HEG, *H. ergaster*; HER, *H. erectus*; HHE, *H. heidelbergensis*; HHA, *H. habilis*; HNE, *H. neanderthalensis*; HSN, *H. sapiens* (North Africa); HSS, *H. sapiens* (sub-Saharan Africa); PAN, *Pan troglodytes*; PBO, *P. boisei*; PRO, *P. robustus*. See text for methodological details and component descriptions

4 | DISCUSSION

These results address the main objectives of this study, which for discussion are divided into three sections: (1) use of the DM-scaled data to characterize hominin species; (2) application of TAS analysis and Bayesian inference to assess how these data differ and distinguish among species; (3) what the variation in relative tooth size indicates about dental evolutionary trends, and why it has potential to elucidate further the phylogeny of *H. naledi* and other hominins. Each point is considered in turn.

4.1 | The data

From a practical standpoint, the DM-RAW scaled data hold several advantages over discrete characters generally employed in hominin research (Strait & Grine, 2004; Smith & Grine, 2008; Berger et al., 2010; Irish et al., 2013; Dembo et al., 2015, 2016; Mongle et al., 2019; also see coding issues in Scotland et al., 2003). Because they are continuous, means based on multiple specimens are used instead of 'typical' characters to represent a species. With a range of standard statistical methods, missing data may also be estimated (e.g., Kenyhercz & Passalacqua, 2016). An absence of empty cells in the present data matrix undoubtedly is a factor in stronger node support than the prior Bayesian hominin trees (Dembo et al., 2015, 2016; Mongle et al., 2019). Crown measurements are reasonably straightforward, and data comparatively unbiased among studies. Observer replicability is a factor like all osteometric recording, but subjective interpretation of characters is minimized. Digital 2D and 3D imaging

methods are even available to enhance precision (Baab et al., 2012; Bernal, 2007; Braga, 2016; Gómez-Robles et al., 2013; Gómez-Robles & Polly, 2012; Hemphill, 2016a; Kato & Ohno, 2009; Mitteroecker & Gunz, 2009), though calipers (used for Table 1) return analogous estimates of linear size and the heritability of phenotype captured (Bernal, 2007; Hlusko et al., 2002).

Further, beyond simply reflecting relative size, the phylogenetic signal is seemingly sufficient to recover reliable evolutionary relationships (i.e., Figure 4). It could be argued that scaling of data in serially homologous teeth, which act as a unit, make them less subject to homoplasy than other morphological characters; contrarily, perhaps it is independence of the incisors from posterior teeth (Hlusko & Mahaney, 2009) that plays a role. Teeth are certainly less affected by any purported homoiology (Lycett & Collard, 2005; von Cramon-Taubadel, 2009). However, it is more likely related to the relatively few taxa and/or their particular evolutionary pathways. Whatever the explanation(s), the posterior probabilities indicate a single maximum a posteriori tree for each model. Felsenstein (2004: 299) states that, "if the data strongly constrain the trees, then we might find only a few [or one]. ... accounting for most of the probability in the posterior," but "if the data are fairly noisy, there might be millions of different trees."

On the other hand, longstanding phylogenetic guidelines advocate that any utility attributed to the DM-scaled data is counterintuitive. Though derived from highly heritable crown dimensions, at least in humans, it cannot be claimed that the data are independent (Billet & Bardin, 2019; Gómez-Robles & Polly, 2012), especially within the molar class (Evans et al., 2016; Kavanagh et al., 2007; Schroer & Wood, 2015). However, this caveat applies to other morphological, as

well as genetic data (Wiens, 2001; O'Leary et al., 2013; Parins-Fukuchi, 2018a; and above). Second, character number is limited compared to the 'super-matrices' in some studies (Dembo et al., 2016; Mongle et al., 2019; Strait & Grine, 2004), but this is more of an issue with maximum parsimony (Wiens, 2004; Wiens & Hillis, 1996) than Bayesian inference (Felsenstein, 2004: EC.Europa.EU, 2016; also Scotland et al., 2003). Finally, perhaps more problematic, the data are from a single anatomical region—the dental module. Characters from one region may provide a different phylogeny than another (Kay, 2015), so sampling across the skeleton is suggested (Dembo et al., 2016; Kay, 2015). In any case, results dictate the usefulness of data, as expanded upon in the next section.

4.2 | The analyses

As expected, TSA results (Table 3, Figure 3) emulate the prior study for the same species (Irish et al., 2016). This technique was designed for continuous odontometric data, so it yields expedient phenetic affinities. However, it is also a useful bridge to phylogenetic inference. The structure of the first component is highly phylogenetic and identifies the deepest node on a resulting tree, that is, that separating one taxon from all others; the second component separates another taxon from the rest, the third another taxon, and so on (Polly et al., 2013; P. D. Polly, personal communication, 2021). Component loadings (Table 3) quantify characters responsible for clade formation, while the 3D plot (Figure 3) illustrates degrees of relationship interpretable using a neighborhood approach (Guttman, 1954; Kruskal & Wish, 1978). As such, the plot provides an indication of likely clades,

and samples inclined to shift—so-called wildcard taxa (Nixon & Wheeler, 1992). For example, the potential for both *Paranthropus* species to form a separate clade with the strict-clock model (SI Figure S7), but nest with other australopiths under the dated relaxed-clock model (Figure 4; also SI Figure S8) is apparent by their somewhat distinct location in a greater neighborhood of other australopiths, early *Homo*, and *H. naledi* in Figure 3. Similarly, the proximity of four sample pairs, *P. boisei/P. robustus*, *H. naledi/H. habilis*, *H. heidelbergensis/H. neanderthalensis*, and both *H. sapiens* samples, portends why all remain sister taxa across trees, regardless of model.

In brief, the first statistically uncorrelated variable, a.k.a. component, identifies the differences in anterior and posterior tooth size; the second, size in the molar class; and the third, shape variation in three teeth. So the 32 scaled data were reduced to three characters explaining >90% of the variance. The first two account for 86%, which is unsurprising given that phylogenetic correlation is expected to contribute to high proportional variance on the first few components; this correlation is needed when reconstructing a phylogeny (Polly et al., 2013; P. D. Polly, personal communication, 2021). Other patterning is discernable as well, for example, the first component additionally defines UM1 and LP3 shape variation (Table 3; SI Figure S4). The second component reflects influence of the inhibitory cascade (ICM) (Evans et al., 2016; Kavanagh et al., 2007; Polly, 2007; Halliday & Goswami, 2013; Schroer & Wood, 2015), here in both isomeres. Postulating that the LM2 occlusal surface comprises a third of total molar area (Evans et al., 2016; Kavanagh et al, 2007; Schroer & Wood, 2015) (e.g., Figures 1 and 2), the ICM is considered valuable for phylogenetic reconstruction, with M1 < M2 < M3 plesiomorphic in hominins (Schroer & Wood, 2015). Yet, as above, crown areas are
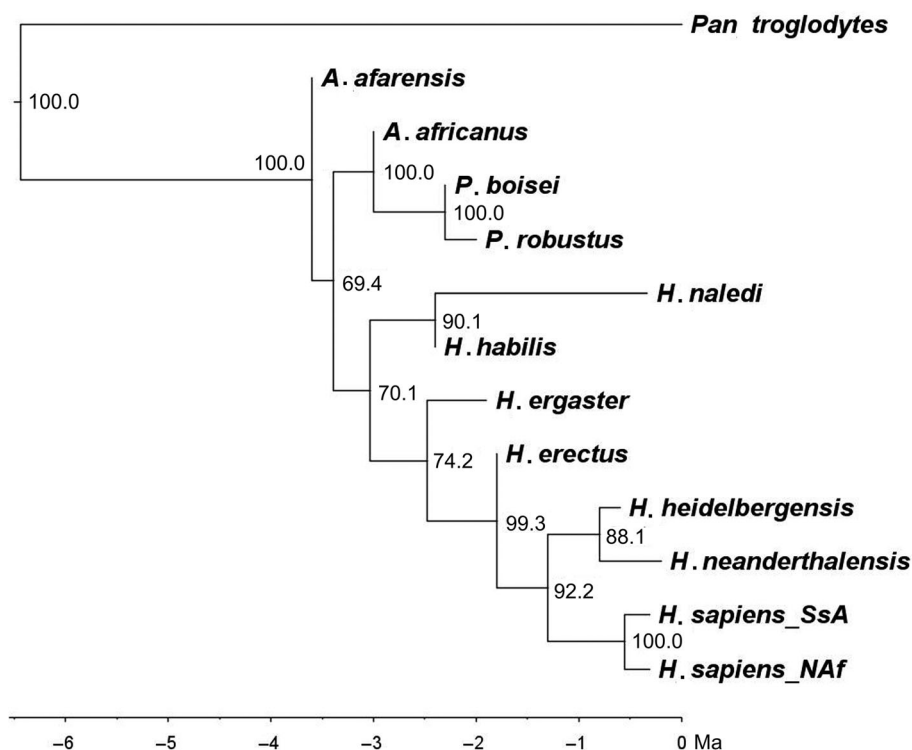

FIGURE 4 Bayesian inference phylogram from dated relaxed-clock analysis based on gap-weighted, DM-scaled data under an MKv model of *H. naledi* and the 12 comparative samples, with clade credibility values for internal nodes included. Scale in millions of years. This is the preferred topology for this study. See text for details

only crude estimates (Garn et al., 1977; Hemphill, 2016a), so more information is represented in this component. Loadings for the DM-scaled MD and BL dimensions suggest some shape differences for the M2, M3, and, noticeably, LP3 (Table 3; SI Figure S5). The same goes for the third component. Accounting for only 4.9% of the variance, its moderate loadings (Table 3; SI Figure S6) imply that *H. naledi* and *H. habilis* have relatively large UI1, UM1, and LI2 MD diameters. This configuration is confirmed for these and other teeth in both species, but only after comparing the 32 DM-scaled data between sample pairs and plotting quotients (SI Figure S9). This is a key factor in differentiating species (below). As a data reduction technique to visualize phenetic variation, the components account for most, but not all phylogenetic signals. Thus, gap-weighted scaled data in Table 2 were used for the phylogenetic analysis.

Overall tree topology does vary across Bayesian models (SI Figures S7 and S8, Figure 4), but as expanded upon below, uniformity in several clades indicates data-driven results. The same clades are also credible as reported in earlier studies, *H. naledi* notwithstanding (Berger et al., 2010; Dembo et al., 2015, 2016; Irish et al., 2013, 2014, 2016, 2018; Mongle et al., 2019; Smith & Grine, 2008; Strait et al., 1997; Strait & Grine, 2004). Those in the strict-clock cladogram (SI Figure S7) resemble the dendrogram clusters (SI Figure S3) for reasons stated. Node support is high, but a polytomy is present, both *Paranthropus* taxa form an outgroup, and *H. ergaster* and *H. erectus* occupy separate clades. Also, at issue is *H. habilis* (and *H. naledi*), in a clade with australopithecines rather than other *Homo* species. Relative to this, the basic relaxed-clock model is favored by Bayes factors. Its tree has greater node support and all australopiths comprise one clade (SI Figure S8). However, it remains unresolved, some taxa shifted, and the two main clades again divide *H. ergaster* and *H. erectus*. These issues might suggest insufficient phylogenetic information (Maddison, 1989; Nixon & Wheeler, 1992; Pol & Escapa, 2009; Purvis & Garland, 1993). Potential factors are model inadequacy, compression of information from the six character-state limit, and/or the data describe nothing beyond the phylogenetic signal of relative tooth size.

The final Bayesian analysis implies that gap-weighted data can recover a plausible phylogenetic hypothesis—under an adequate model. The dated relaxed-clock is strongly favored over the preceding two models. It yielded a fully-resolved tree, very strong node support, and a credible topology (Figure 4). Aside from *H. naledi* (i.e., Dembo et al., 2016), the calibrated phylogram is congruent with those from prior Bayesian inference (Dembo et al., 2015; Mongle et al., 2019), and the preferred trees from maximum parsimony (Mongle et al., 2019; Smith & Grine, 2008; Strait et al., 1997; Strait & Grine, 2004). With this model any compromised signal from low state number was likely improved by two factors. First, a relaxed-clock is recommended for comparing different species, with a prior distribution of evolutionary rates that vary among the taxa and branches (Felsenstein, 2004; Pybus, 2006). Second, the fossilized birth-death prior promotes unrestricted variation in branch length. To illustrate, an earlier dated relaxed-clock analysis using the default priors of equal rates and uniform branch lengths, yielded a phylogram with highly

inaccurate branch variation relative to divergence times (SI Figure S10); clades are identical to those from the basic relaxed clock model, including the same two polytomies (SI Figure S8).

To test further the dated FBD model, *Ardipithecus ramidus* and *A. anamensis* were added after the above analyses were completed (not shown). Data are available for these species (details in SI Table S4), but they do not meet the second criterion for original sample selection—multiple MD and BL measurements for all teeth. However, by adding these older species (4.5 and 4.2 Ma FAD, respectively; Du et al., 2020) the branch length to the root was shortened; long branch lengths can unduly bias locations of the remaining taxa (Felsenstein, 2004). The resulting calibrated phylogram, presented in Figure 5, is otherwise identical to Figure 4. Other than *H. naledi* it is also fully congruent with prior studies, notably Dembo et al. (2016). On these bases, the calibrated model yields the preferred a posteriori hypothesis to explore relative tooth size variation in *H. naledi* and other hominins, after first discussing the implications of the uncalibrated results.

4.3 | The phylogenies of relative tooth size

Cladograms from the two uncalibrated Bayesian models are comparable (SI Figures S7 and S8; also SI Figure S3), with exceptions noted. Focusing on the favored of these two, the primary clades evident in the basic relaxed-clock topology consist of: (1) *P. robustus*, *P. boisei*, *A. africanus*, *A. afarensis*, *H. habilis*, *H. ergaster*, and *H. naledi*—all of African origin and, other than the latter, the oldest species at 3.6–1.9 Ma FAD, versus (2) the succeeding four *Homo* species of non-African or recent origin, dating 1.8 Ma FAD to present. These are incongruent with accepted phylogenies, but distinguish dental evolutionary trends across both space and time, such as the inhibitory cascade (ICM) (also see PC2 in Figure 3). Again, species in the first clade are characterized by M1 < M2 < M3; those in the second trend toward or exhibit the M1 > M2 > M3 gradient. But, as noted, size based on molar crown areas is only part of the variation. If it is assumed australopithecines are ancestral to the remaining species in this study, two other trends are indicated. First, DM-scaled MD and BL dimensions increased equivalently to yield relatively larger postcanine teeth of *P. robustus* and *P. boisei* (Table 2, Figure 2). Second, In *H. habilis* these teeth are generally reduced but, importantly, in scaled BL size more than MD to result in relatively long, narrow posterior teeth as described here. Additional teeth in the species show similar unequal reduction in scaled size (also PC3 in Figure 3). This pattern is retained in the overall smaller teeth of *H. ergaster*, but intensified in *H. naledi*, as detailed below. These trends may be gleaned from Table 2, but are succinctly illustrated by plotting scaled dimensions of the LM2 (Figure 6), that is, the central tooth of the molar ICM (also see plots of between-sample quotients in SI Figure S9, as discussed below). The three African *Homo* species all lie below the reference line of the LM2 graph, with a long DM-scaled MD dimension relative to BL. The remaining nine samples, on or above this line, have an LM2 ranging from relatively proportional to short and wide in shape.

FIGURE 5 Bayesian inference phylogram from dated relaxed-clock analysis based on gap-weighted, DM-scaled data under an MKv model of *H. naledi*, the 12 comparative samples, plus *Ardipithecus ramidus* (4.5 ma FAD) and *A. anamensis* (4.2 ma FAD) to further test the model, and shorten branch length to the root. Clade credibility values for internal nodes are included. Scale in millions of years. See text for details
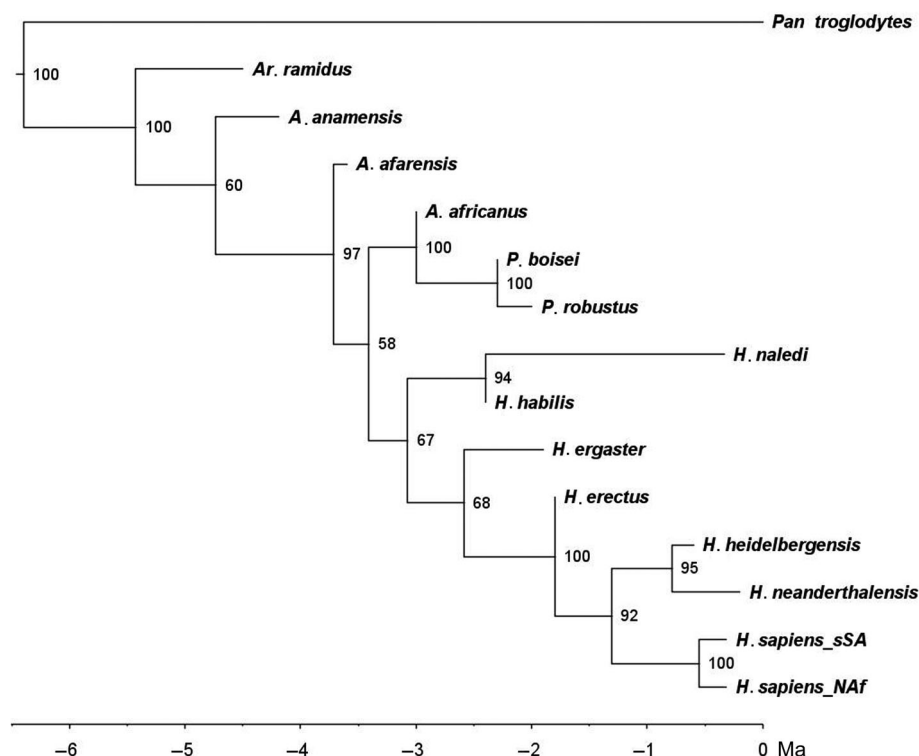

FIGURE 6 Scatterplot of DM-scaled MD and BL dimensions of the LM2—central tooth of the Inhibitory Cascade Model—with fit line at the total as reference to summarize relative postcanine tooth size variation among the 12 hominin samples. AFA, *A. afarensis*; AFR, *A. africanus*; HEG, *H. ergaster*; HER, *H. erectus*; HHA, *H. habilis*; HHE, *H. heidelbergensis*; HNE, *H. neanderthalensis*; HSN, *H. sapiens* (North Africa); HSS, *H. sapiens* (sub-Saharan Africa); PAN, *Pan troglodytes*; PBO, *P. boisei*; PRO, *P. robustus*. See text for details
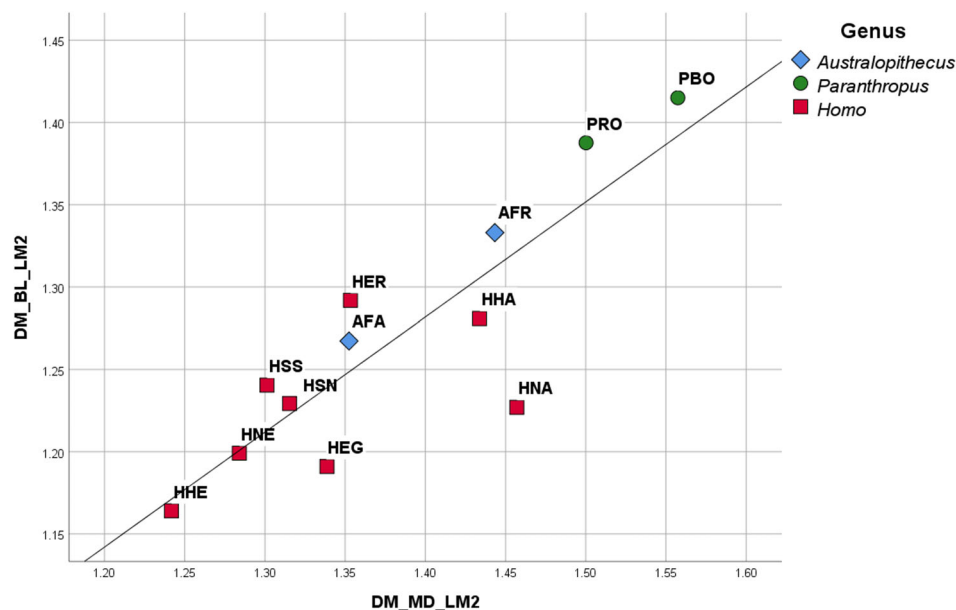
Numerous diet-related hypotheses have been proposed to explain the postcanine megadontia of *Paranthropus* (overview in Wood & Patterson, 2020), and the opposite in *Homo*, though most of the latter consider extra oral processing of food rather than direct consumption (overview in Veneziano et al., 2019). But what explains the shape differences seen in more ancient African *Homo* versus non-African and recent *Homo* species—most notably between *H. ergaster* and *H. erectus* (before application of the calibrated FBD model)? *Homo erectus* is characterized by (re)expansion of scaled BL dimensions relative to MD (Table 2), as again visualized using the LM2 (Figure 6).

Succeeding *Homo* species evidence a decrease in overall crown size, but with more marked scaled MD reduction, to reach the extreme seen in *H. sapiens*. This trend is evidenced by the location of the latter, between *H. erectus* to the right along the reference line, and *H. neanderthalensis* and *H. heidelbergensis* on the left—as characterized by more equivalent reduction of the two scaled dimensions. Is it indeed BL expansion in non-African *H. erectus*—from which the subsequent *Homo* species evolved? Or, despite contrary data (Table 2), is it a more parsimonious explanation, that is, MD decrease from reduced jaw size (Veneziano et al., 2019)? Further study into the reason(s)

driving this trend, reported here for the first time, is warranted concerning shifts in environment, diet, and/or behavior, to yield the dentitions of *H. erectus* and its descendants.

Turning to the preferred calibrated phylogram (Figure 4; also Figure 5), the discussion now focuses on *H. naledi*. It seems that a common supposition (Greshko, 2017), with minimal published support, is that the species is directly descended from African *H. erectus* (i.e., *H. ergaster*). Yet, in the original article, Berger et al. (2015) described only what was considered enough similarities with several *Homo* species, including *H. erectus*, to warrant classification in the genus. Using published craniometric data Thackeray (2015) agreed, though he also found *H. naledi* to be most like *H. habilis*, and to a lesser extent *H. ergaster*. Overall, prior comparisons of crania and postcrania indicate *H. naledi* has *Homo*- and *Australopithecus*-like features. Examples include a well-developed, arched supraorbital torus separated from the vault by a continuous supra-toral sulcus like in *H. habilis* and *H. erectus*, marked angular and occipital tori like *H. erectus*, and some facial similarities to *H. rudolfensis* (Berger et al., 2015; Hawks et al., 2017; Schroeder et al., 2017). Cranially, it is nothing like recent *Homo*—seen in its endocranial morphology (Holloway et al., 2018) and *Australopithecus*-like cranial capacity (Garvin et al., 2017). In the postcrania, *Homo*-like traits include long tibiae and gracile fibulae, muscle attachments that suggest a striding gate, and modern features in the ankles, feet, and hands. *Australopithecus*-like features include curved phalanges (also in *H. habilis*), a wide lower thorax, ape-like arms, primitive pelvic morphology, and the same for certain aspects of the femur (Berger et al., 2015; Feuerriegel et al., 2017; Garvin et al., 2017; Harcourt-Smith et al., 2015; Hawks et al., 2017; Kivell et al., 2015; Marchi et al., 2017; VanSickle et al., 2018; Williams et al., 2016).

This mosaic of plesiomorphic, apomorphic, and apparent autapomorphic characters affected the prior attempt at Bayesian inference by Dembo et al. (2016). In their phylogram *H. naledi* is nested within a clade of 11 *Homo* species and *A. sediba*, but its position therein is ambiguous. The species cannot be excluded as a sister taxon to any one of several clade members, including *H. antecessor*, *H. erectus/ergaster*, *H. habilis*, *H. floresiensis*, and *H. sapiens*, among others. Node support between *H. naledi* and a smaller clade containing *H. antecessor*, *H. sapiens*, and the sister taxa *H. heidelbergensis* and *H. neanderthalensis*, is only 36%. Other clade credibility values leading to the latter node range between 21–54% (Dembo et al., 2016). A phenetic comparison of dental morphological traits also found *H. naledi* to group nearest *H. habilis* and *H. ergaster*; however, the unique combinations and expressions of traits differ enough to support its taxonomic status as a separate species in the genus (Irish et al., 2018). As well, the species' molar root metrics revealed similarities with individual specimens of *H. habilis* (KNM-ER 1805), *H. ergaster* (SK 15), and early *Homo* sp. (SK 45) (Kupczik et al., 2019).

Most recently, research into dental similarities of *H. naledi* with other hominins has tacked toward *Paranthropus*. The deciduous mandibular canine and the first molars in both isomeres share apparent derived traits with the latter genus, though features of the second deciduous molars are *Homo*-like (Bailey et al., 2019). In a geometric morphometric study of mandibular premolar enamel-dentine junctions (EDJ), Davies et al. (2020) reported that the species *is* closest to *P. robustus* in a PCA ordination of the first two components (73.7% of variation) for LP3 shape. *Homo habilis* is plotted nearby, but other specimens in the genus, including *H. erectus* and, in particular, *H. neanderthalensis* and *H. sapiens*, are increasingly distinct. That said, their third component (6.4% of the variation) of LP3 shape separates *H. naledi* and *P. robustus*, as do analyses of LP4 EDJ morphology and the centroid sizes of both premolars. From this, the authors maintain that the suite of traits is distinguishable from other hominin specimens in their analysis, including most early and later *Homo* species.

Cranial, dental, and postcranial features offer conflicting evidence for the place of *H. naledi* in hominin evolution—though with enough agreement to assign it to genus. Here, the DM-scaled data link the species to *H. habilis* though, again, sample size must be considered. Despite the method employed, both remain sister taxa with strong node support of >75–90%. The latter value is from the dated relaxed-clock phylogram in Figure 4; it reaches 94% in the expanded calibrated analysis with *Ar. ramidus* and *A. anamensis* (Figure 5). Of interest, when not nested among older African-only species in the uncalibrated trees (SI Figures S7 and S8; also Figure S3), it and *H. habilis* are in a clade most proximate to them with the preferred model.

Returning to how size is apportioned along dental rows, *H. naledi* and other African *Homo* and *Australopithecus* species are characterized by general uniformity relative to the extreme opposing patterns in *Pan troglodytes* and *Paranthropus* (Tables 2 and 3, Figure 3 PC1). Contra *Pan*, *H. naledi* has smaller anterior and larger posterior teeth. On an individual basis, other than *Pan*'s sectorial LP3, the teeth of *H. naledi* also have relatively larger DM-scaled MD than BL diameters (SI Figure S9(a)). A pattern contrary to highly derived *P. robustus* and *P. boisei* would be expected in *H. naledi*, namely, larger anterior and smaller posterior teeth. This pattern is evident, but enough scaled dimensions are similar to *Paranthropus*, notably *P. robustus* (Table 2), that exceptions occur. The UM1s are equivalent in relative size across these species, as are DM-scaled MD dimensions of the UP3, UM2, LM1, and LM2, and DM-scaled BL equivalents of the UI1, LI1, LC, and LM3 (SI Figure S9(b,c)). Again, as with *Pan*, the *H. naledi* teeth are comparatively longer in DM-scaled MD dimensions than, in this instance, the buccolingually larger teeth of *Paranthropus*.

The apportionment of tooth size in *H. naledi* is most similar to that of *H. habilis* and, to a lesser degree, *A. africanus* and *A. afarensis*. Other than the general uniformity in DM-scaled anterior and posterior dentition size, all share a strong M1 < M2 < M3 gradient relative to the ICM (Schroer and Wood, 2015). As well, molars and several other teeth are of similar relative size among the species. In fact, in ICM proportions, Evans et al. (2016) found that *H. habilis* is more like the australopiths than other early *Homo* species, which would not be unexpected in a putatively basal member of the latter genus. This finding prompted these authors to cite a paper suggesting the taxon could be *Australopithecus habilis* (Wood & Collard, 1999). In any event, a number of scaled dimensions distinguish *H. naledi* from the australopithecines. The former has a noticeably smaller LC, but comparatively

large scaled UI2, LI1, and LI2 MD dimensions —particularly in contrast to *A. africanus* (SI Figure S9(d–f)). Though less marked than *Pan* (see above), the scaled MD dimension of the *H. naledi* LP3 is also large versus the BL, as indicated by the associated loading in Table 3. *Homo naledi* can be differentiated from *H. habilis* on these bases to some extent, but their symplesiomorphies are more obvious. As indicated, they are the only two species with an LP3 that is not wider (BL) than it is long (MD) (Table 1). In fact, teeth in both species are characterized by large DM-scaled MD dimensions relative to all australopiths (Tables 2 and 3, Figure 3 PC2 and PC3). Beyond the shared molar size gradient, *H. naledi* and *H. habilis* have long, narrow posterior teeth noted above (also SI Figure S9(f)), unlike derived recent *Homo* with mesiodistally reduced premolars and molars (SI Figure S9(g–l)). However, anterior teeth of the latter *Homo* species are relatively larger in both isomeres, particularly the BL dimensions, than *H. naledi* or *H. habilis*.

Based on these characters, which link *H. naledi* to the most ancient *Homo* species included in the present study, *H. naledi* has a plesiomorphic pattern of size apportionment. Of course, this inference again assumes ancestry of *Australopithecus* to *H. habilis*, which in turn is a basal member in its assigned genus. Other researchers made similar statements for alternate skeletal structures. Schroeder et al. (2017) report that while certain cranial traits ally *H. naledi* with *H. erectus*, those of the mandible are more like basal *Homo*. Holloway et al. (2018:5741) state that "derived aspects of endocranial morphology in *H. naledi* were likely present in the common ancestor of the genus." And, Davies et al. (2020) suggest that several derived morphological features of the premolars shared by *H. naledi* and [African] *H. erectus*, are homoplastic, evolving independently in both from a basal *Homo* condition like *H. habilis*. They conclude by proposing "*H. naledi* represents a long surviving lineage that split from other members of the genus *Homo* relatively early" (Davies et al., 2020:13196.9). The present results support this inference and others finding links to a common, and early, *Homo* condition. That said, the phylogenetic place of *H. naledi* is clearly a work in progress. More remains are being recovered, but of greater importance to increase understanding is the discovery of specimens older than the age of the Dinaledi chamber; as implied by the above findings, they should be present. As/if more ancient *H. naledi* remains are found it should be possible, ideally in combination with characters from multiple anatomical regions, to discern just how long this potentially long surviving lineage survived, alongside or in the shadow of several successive hominin species, including *H. sapiens*.

5 | SUMMARY AND CONCLUSIONS

The DM_RAW correction from Jungers et al. (1995) was used to equivalently scale 32 MD and BL measurements in *H. naledi* and 12 other Plio-Pleistocene and recent samples: *A. africanus*, *A. afarensis*, *P. robustus*, *P. boisei*, *H. habilis*, *H. ergaster*, *H. erectus*, *H. heidelbergensis*, *H. neanderthalensis*, two samples of *H. sapiens*, and *Pan troglodytes*.

One aim was to provide further morphological characterization of the recently discovered South African hominin. The DM-scaled data were employed in an approach called TSA analysis to assess intersample phenetic affinities (Irish et al., 2016). Then, after quantitative coding, the 32 scaled characters were used in Bayesian inference. Yet, whether 3D ordination or phylogenetic tree, and irrespective of Bayesian priors, the comparability in several key clades implies data-driven results. The results identify effects of presumed evolutionary trends on relative tooth size across species, beyond that previously reported. Then, using the relaxed-clock model to permit variation in evolutionary rates and, importantly, gamma rates and fossilized birth-death priors for unrestricted branch length variation, the final dated analysis yielded a tree congruent with prior phylogenetic studies. Under an appropriate Bayesian model the implication is that, beyond reflecting information about relative tooth size, these data can recover plausible evolutionary relationships.

With regard to *H. naledi*, the species forms a clade with *H. habilis* as a sister taxon. It also shares similarities with older African species that, based on published dates, range between 3.6 to 1.9 Ma FAD, including: *A. afarensis*, *A. africanus*, *H. habilis* and *H. ergaster*. *Homo naledi* (and *H. habilis*) is an outgroup to other potentially contemporaneous *Homo* taxa, *H. erectus*, *H. neanderthalensis*, and *H. sapiens*, in support of several recent studies based on comparisons of other skeletal features. *Homo naledi* has a plesiomorphic pattern of TSA, like the oldest species in this study. This basal *Homo* condition implies that the origin of *H. naledi* predates the ∼335–236 ka age of the Dinaledi Chamber from which the original fossils were recovered (Dirks et al., 2017). The species may indeed represent a long-lived side branch in the genus *Homo*, perhaps rivaling *H. habilis* or another basal species in age, while persisting until the advent of *H. sapiens*.

Finally, though limited to one anatomical region and lacking proof of independence, the DM-scaled data, with an appropriate model, warrant consideration for future hominin phylogenetic research. This approach would preferably entail combining them with other quantitative and/or more traditional discrete characters from multiple anatomical regions to yield a larger character matrix. Moreover, DM-scaled data are candidates for use in their original continuous form (Table 2). Recent advances in probabilistic phylogenetics, notably Bayesian inference, allow use of models, for example, Brownian motion, capable of approximating evolution of continuous morphological characters (Felsenstein, 2004; Parins-Fukuchi, 2018a, 2018b). Beyond objective data recording as mentioned, continuous data do not require the ordering of states, and should retain phylogenetic information at much higher evolutionary rates than coded characters—qualitative or quantitative—because they do not necessitate compression into a limited number of states (Parins-Fukuchi, 2018a, 2018b). Initial results using this approach with the current dataset (Table 2) and hominin taxa appear promising; analyses are ongoing.

32 generated independent randomly evolving characters and calculations of variance to reaffirm for us "...that the amount of variance explained by the first [few] PCs may have nothing to do with inter-trait correlations and everything to do with phylogenetic topology." Thank you to everyone who is currently or formerly affiliated with the institutions at which the North and sub-Saharan *H. sapiens* odontometric measurements were recorded: Charles Merbs and Donald Morris, Arizona State University (ASU); Elden Johnson, University of Minnesota; Douglas Ubelaker, David Hunt, and Carol Butler, National Museum of Natural History; Ian Tattersall, Jaymie Brauer, and Gary Sawyer, American Museum of Natural History; Andre Langaney, Frances Roville-Sausse, and Miya Awazu Periera da Silva, Musée de l'Homme; Romuald Schild, Michal Kobusiewicz, and Jacek Kabaciński, Combined Prehistoric Expedition to Gebel Ramlah; and Renée Friedman, Hierakonpolis Expedition. Thanks are extended to Lee Berger, from theCentre for the Exploration of the Deep Human Journey; Darryl de Ruiter, Texas A&M, for measurements in our 2016 publication incorporated here; Lucas Delezene, University of Arkansas, who provided a list of publications with Asian *H. erectus* MD and BL measurements, several of which were accessed for the summary data. Funding for data collection by the first author came from the National Science Foundation (BNS-9013942), the ASU Research Development Program, and the American Museum of Natural History.

CONFLICT OF INTEREST

This statement is to certify that the authors have no conflict of interest to declare.

AUTHOR CONTRIBUTIONS

Joel Irish: Conceptualization; data curation; formal analysis; funding acquisition; investigation; methodology; project administration; resources; software; supervision; validation; visualization; writing-original draft; writing-review & editing. **Mark Grabowski:** formal analysis; investigation; methodology; resources; software; validation; visualization; writing-review & editing.

DATA AVAILABILITY STATEMENT

The odontometric data used in the analyses are available in the text (Tables 1-2) and in the supporting information file.

ORCID

Joel D. Irish https://orcid.org/0000-0001-7857-8847

REFERENCES

Adams, D. C., & Felice, R. N. (2014). Assessing trait covariation and morphological integration on phylogenies using evolutionary covariance matrices. *PloS One*, 9(4), e94335.

Alvesalo, L., & Tigerstedt, P. M. A. (1974). Heritabilities of human tooth dimensions. *Hereditas*, 77, 311–318.

Amster, G., & Sella, G. (2016). Life history effects on the molecular clock of autosomes and sex chromosomes. *Proceedings of the National Academy of Sciences*, 113(6), 1588–1593.

Antón, S. C., Potts, R., & Aiello, L. C. (2014). Evolution of early *Homo*: An integrated biological perspective. *Science*, 345(6192), 1236828.

Baab, K. L., McNulty, K. P., & Rohlf, F. J. (2012). The shape of human evolution: A geometric morphometrics perspective. *Evolutionary Anthropology: Issues, News, and Reviews*, 21(4), 151–165.

Bailey, S. E., Brophy, J. K., Moggi-Cecchi, J., & Delezene, L. K. (2019). The deciduous dentition of *Homo naledi*: A comparative study. *Journal of human evolution*, 136, 102655.

Baydaş, B., Oktay, H., & Metin Dağsuyu, İ. (2005). The effect of heritability on Bolton tooth-size discrepancy. *The European Journal of Orthodontics*, 27(1), 98–102.

Berger, L. R., De Ruiter, D. J., Churchill, S. E., Schmid, P., Carlson, K. J., Dirks, P. H., & Kibii, J. M. (2010). *Australopithecus sediba*: A new species of *Homo*-like australopith from South Africa. *Science*, 328(5975), 195–204.

Berger, L. R., Hawks, J., de Ruiter, D. J., Churchill, S. E., Schmid, P., Delezene, L. K., Kivell, T. L., Garvin, H. M., Williams, S. A., DeSilva, J. M., Skinner, M. M., Musiba, C. M., Cameron, N., Holliday, T. W., Harcourt-Smith, W., Ackermann, R. R., Bastir, M., Bogin, B., Bolter, D., ... Zipfel, B. (2015). *Homo naledi*, a new species of the genus *Homo* from the Dinaledi chamber, South Africa. *eLife*, 4, e09560.

Bermúdez de Castro, J. M. (1986). Dental remains from Atapuerca (Spain) I. Metrics. *Journal of Human Evolution*, 15(4), 265–287.

Bernal, V. (2007). Size and shape analysis of human molars: Comparing traditional and geometric morphometric techniques. *Homo*, 58(4), 279–296.

Billet, G., & Bardin, J. (2019). Serial homology and correlated characters in morphological phylogenetics: Modeling the evolution of dental crests in placentals. *Systematic Biology*, 68(2), 267–280.

Braga, J. (2016). Non-invasive imaging techniques. In J. D. Irish & G. R. Scott (Eds.), *A companion to dental anthropology* (pp. 514–527). Wiley-Blackwell.

Collard, M., & Wood, B. (2000). How reliable are human phylogenetic hypotheses? *Proceedings of the National Academy of Sciences*, 97(9), 5003–5006.

Corruccini, R. S. (1973). Size and shape in similarity coefficients based on metric characters. *American Journal of Physical Anthropology*, 38(3), 743–753.

Darroch, J. N., & Mosimann, J. E. (1985). Canonical and principal components of shape. *Biometrika*, 72(2), 241–252.

Davies, T. W., Delezene, L. K., Gunz, P., Hublin, J. J., Berger, L. R., Gidna, A., & Skinner, M. M. (2020). Distinct mandibular premolar crown morphology in *Homo naledi* and its implications for the evolution of *Homo* species in southern Africa. *Scientific reports*, 10(1), 1–13.

Dembo, M., Matzke, N. J., Mooers, A. Ø., & Collard, M. (2015). Bayesian analysis of a morphological supermatrix sheds light on controversial fossil hominin relationships. *Proceedings of the Royal Society B: Biological Sciences*, 282(1812), 20150943.

Dembo, M., Radovčić, D., Garvin, H. M., Laird, M. F., Schroeder, L., Scott, J. E., Brophy, J., Ackermann, R. R., Musiba, C. M., de Ruiter, D. J., & Collard, M. (2016). The evolutionary relationships and age of *Homo naledi*: An assessment using dated Bayesian phylogenetic methods. *Journal of Human Evolution*, 97, 17–26.

Dempsey, P. A., & Townsend, G. C. (2001). Genetic and environmental contributions to variation in human tooth size. *Heredity*, 86(6), 685–693.

Dempsey, P. J., Townsend, G. C., Martin, N. G., & Neale, M. C. (1995). Genetic covariance structure of incisor crown size in twins. *Journal of Dental Research*, 74(7), 1389–1398.

Devièse, T., Karavanić, I., Comeskey, D., Kubiak, C., Korlević, P., Hajdinjak, M., Radović, S., Procopio, N., Buckley, M., Pääbo, S., & Higham, T. (2017). Direct dating of Neanderthal remains from the site of Vindija cave and implications for the middle to upper Paleolithic transition. *Proceedings of the National Academy of Sciences*, 114(40), 10606–10611.

Dirks, P., Roberts, E. M., Hilbert-Wolf, H., Kramers, J. D., Hawks, J., Dosseto, A., Duval, M., Elliott, E. M., Grün, R., Hellstrom, J.,

Herries, A. I. R., Joannes-Boyau, R., Placzek, C. J., Robbins, J., Spandler, C., Wiersma, J., Woodhead, J., & Berger, L. R. (2017). The age of *Homo naledi* and associated sediments in the rising star cave, South Africa. *eLife*, *6*, e24231.

Du, A., Rowan, J., Wang, S. C., Wood, B. A., & Alemseged, Z. (2020). Statistical estimates of hominin origination and extinction dates: A case study examining the *Australopithecus anamensis–afarensis* lineage. *Journal of human evolution*, *138*, 102688.

Du, A., Zipkin, A. M., Hatala, K. G., Renner, E., Baker, J. L., Bianchi, S., Bernal, K. H., & Wood, B. A. (2018). Pattern and process in hominin brain size evolution are scale-dependent. *Proceedings of the Royal Society B: Biological Sciences*, *285*(1873), 20172738.

EC.Europa.EU, (2016). Bayesian phylogenetics using MrBayes and RevBayes https://ec.europa.eu/research/participants/documents/downloadPublic/TFRocTArcjZRczduMW9LWmRJUm1UL0RXckVPSjFlZGNMcE5mWkUvbWErWHAyenBXMkZNNk1BPT0=/attachment/VFEyQTQ4M3ptUWY1Z0NCT2xUa2JUb0dCCMmpyMlZSTE8.

Evans, A. R., Daly, E. S., Catlett, K. K., Paul, K. S., King, S. J., Skinner, M. M., Nesse, H. P., Hublin, J. J., Townsend, G. C., Schwartz, G. T., & Jernvall, J. (2016). A simple rule governs the evolution and development of hominin tooth size. *Nature*, *530*(7591), 477–480.

Farris, J. S. (1983). The logical basis of phylogenetic analysis. *Advances in Cladistics.*, *2*, 7–36.

Felsenstein, J. (1985). Confidence-limits on phylogenies–an approach using the bootstrap. *Evolution*, *39*, 783–791.

Felsenstein, J. (2002). Quantitative characters, phylogenies and morphometrics. In N. MacLeod & P. L. Forey (Eds.), *Morphology, shape and phylogeny* (pp. 27–44). CRC Press.

Felsenstein, J. (2004). *Inferring phylogenies*. Sinauer Associates.

Feuerriegel, E. M., Green, D. J., Walker, C. S., Schmid, P., Hawks, J., Berger, L. R., & Churchill, S. E. (2017). The upper limb of *Homo naledi*. *Journal of Human Evolution*, *104*, 155–173.

Garcia-Cruz, J., & Sosa, V. (2006). Coding quantitative character data for phylogenetic analysis: A comparison of five methods. *Systematic Botany*, *31*(2), 302–309.

Garn, S. M., Brace, C. L., & Cole, P. E. (1977). Use of crown areas in odontometric analyses. *Journal of Dental Research*, *56*, 876.

Garvin, H. M., Elliott, M. C., Delezene, L. K., Hawks, J., Churchill, S. E., Berger, L. R., & Holliday, T. W. (2017). Body size, brain size, and sexual dimorphism in *Homo naledi* from the Dinaledi chamber. *Journal of Human Evolution*, *111*, 119–138.

Gibbon, R. J., Pickering, T. R., Sutton, M. B., Heaton, J. L., Kuman, K., Clarke, R. J., Brain, C. K., & Granger, D. E. (2014). Cosmogenic nuclide burial dating of hominin-bearing Pleistocene cave deposits at Swartkrans, South Africa. *Quaternary Geochronology*, *24*, 10–15.

Goloboff, P. A., Mattoni, C. I., & Quinteros, A. S. (2006). Continuous characters analyzed as such. *Cladistics*, *22*(6), 589–601.

Gómez-Robles, A., de Castro, J. M. B., Arsuaga, J. L., Carbonell, E., & Polly, P. D. (2013). No known hominin species matches the expected dental morphology of the last common ancestor of Neanderthals and modern humans. *Proceedings of the National Academy of Sciences*, *110*(45), 18196–18201.

Gómez-Robles, A., & Polly, P. D. (2012). Morphological integration in the hominin dentition: Evolutionary, developmental, and functional factors. *Evolution: International Journal of Organic Evolution*, *66*(4), 1024–1043.

Greshko, M. (2017). Did This Mysterious Ape-Human Once Live Alongside Our Ancestors? https://www.nationalgeographic.com/news/2017/05/homo-naledi-human-evolution-science/.

Guillerme, T., & Brazeau, M. D. (2018). Influence of different modes of morphological character correlation on phylogenetic tree inference. *BioRxiv*, *308742*, 1–44.

Guttman, L. (1954). Some necessary conditions for common-factor analysis. *Psychometrika*, *19*, 149–161.

Halliday, T. J., & Goswami, A. (2013). Testing the inhibitory cascade model in Mesozoic and Cenozoic mammaliaforms. *BMC Evolutionary Biology*, *13*(1), 1–11.

Harcourt-Smith, W., Throckmorton, Z., Congdon, K., Zipfel, B., Deane, A. S., Drapeau, M., Churchill, S., Berger, L., & DeSilva, J. (2015). The foot of *Homo naledi*. *Nature Communications*, *6*, 8432.

Harris, E. F. (1997). A strategy for comparing odontometrics among groups. *Dental Anthropology*, *12*, 1–6.

Harris, E. F. (1998). Ontogenetic and intraspecific patterns of odontometric associations in humans. In J. R. Lukacs (Ed.), *Human dental development, morphology, and pathology: A tribute to Albert A. Dahlberg* (pp. 299–346). University of Oregon Anthropological Papers.

Harris, E. F. (2003). Where's the variation? Variance components in tooth sizes of the permanent dentition. *Dental Anthropology*, *16*, 84–94.

Harris, E. F., & Bailit, H. L. (1988). A principal components analysis of human odontometrics. *American Journal of Physical Anthropology*, *75*(1), 87–99.

Harris, E. F., & Rathbun, T. A. (1991). Ethnic differences in apportionment of tooth sizes. In M. A. Kelley & C. S. Larsen (Eds.), *Advances in dental anthropology* (pp. 121–142). Alan R Liss.

Harris, E. F., & Harris, J. T. (2007). Racial differences in tooth crown size gradients within morphogenetic fields. *Revista Estomatología*, *15*(3), 7–16.

Hawks, J., Elliott, M., Schmid, P., Churchill, S. E., de Ruiter, D. J., Roberts, E. M., Hilbert-Wolf, H., Garvin, H. M., Williams, S. A., Delezene, L. K., Feuerriegel, E. M., Randolph-Quinney, P., Kivell, T. L., Laird, M. F., Tawane, G., DeSilva, J. M., Bailey, S. E., Brophy, J. K., Meyer, M. R., ... Berger, L. R. (2017). New fossil remains of *Homo naledi* from the Lesedi chamber, South Africa. *eLife*, *6*, e24232.

Heath, T. A. (2015). Divergence time estimation using BEAST v2. 2.0. In *Tutorial written for workshop on applied phylogenetics and molecular evolution* (pp. 1–44). Bodega Bay California. http://treethinkers.org/tutorials/divergence-time-estimation-using-beast/

Heath, T. A., Huelsenbeck, J. P., & Stadler, T. (2014). The fossilized birth–death process for coherent calibration of divergence-time estimates. *Proceedings of the National Academy of Sciences*, *111*(29), E2957–E2966.

Hedges, S. B., & Kumar, S. (2009). Introduction. In S. B. Hedges & S. Kumar (Eds.), *Discovering the timetree of life* (pp. 3–86). Oxford University Press.

Hemphill, B. E. (2016a). Measurement of tooth size (odontometrics). In J. D. Irish & G. R. Scott (Eds.), *A companion to dental anthropology* (pp. 287–310). Wiley-Blackwell.

Hemphill, B. E. (2016b). Assessing odontometric variation among populations. In J. D. Irish & G. R. Scott (Eds.), *A companion to dental anthropology (pp. 311–336)*. Wiley-Blackwell.

Hemphill, B. E., Lukacs, J. R., & Rami Reddy, V. (1992). Tooth size apportionment among contemporary Indians: Factors of caste, language, and geography. *Journal of Human Ecology*, *2*, 231–253.

Herries, A. I., & Adams, J. W. (2013). Clarifying the context, dating and age range of the Gondolin hominins and *Paranthropus* in South Africa. *Journal of Human Evolution*, *65*(5), 676–681.

Herries, A. I., Pickering, R., Adams, J. W., Curnoe, D., Warr, G., Latham, A. G., & Shaw, J. (2013). A multi-disciplinary perspective on the age of *Australopithecus* in southern Africa. In K. Reed, J. G. Fleagle, & R. E. Leakey (Eds.), *The paleobiology of Australopithecus* (pp. 21–40). Springer.

Hlusko, L. J., & Mahaney, M. C. (2009). Quantitative genetics, pleiotropy, and morphological integration in the dentition of *Papio hamadryas*. *Evolutionary Biology*, *36*(1), 5–18.

Hlusko, L. J., Weiss, K. M., & Mahaney, M. C. (2002). Statistical genetic comparison of two techniques for assessing molar crown size in pedigreed baboons. *American Journal of Physical Anthropology*, *117*(2), 182–189.

Hlusko, L. J., Schmitt, C. A., Monson, T. A., Brasil, M. F., & Mahaney, M. C. (2016). The integration of quantitative genetics, paleontology, and neontology reveals genetic underpinnings of primate dental evolution. *Proceedings of the National Academy of Sciences*, 113(33), 9262–9267.

Holloway, R. L., Hurst, S. D., Garvin, H. M., Schoenemann, P. T., Vanti, W. B., Berger, L. R., & Hawks, J. (2018). Endocast morphology of *Homo naledi* from the Dinaledi chamber, South Africa. *Proceedings of the National Academy of Sciences*, 115(22), 5738–5743.

Huelsenbeck, J. P., & Ronquist, F. (2001). MRBAYES: Bayesian inference of phylogenetic trees. *Bioinformatics*, 17(8), 754–755.

Irish, J. D. (2005). Population continuity vs. discontinuity revisited: Dental affinities among late Paleolithic through Christian-era Nubians. *American Journal of Physical Anthropology*, 128(3), 520–535.

Irish, J. D. (1993). *Biological affinities of late Pleistocene through modern African aboriginal populations: The dental evidence*. Dissertation, Arizona State University, Tempe.

Irish, J. D. (2000). The Iberomaurusian enigma: North African progenitor or dead end? *Journal of Human Evolution*, 39(4), 393–410.

Irish, J. D. (2006). Who were the ancient Egyptians? Dental affinities among Neolithic through postdynastic peoples. *American Journal of Physical Anthropology*, 129(4), 529–543.

Irish, J. D. (2008). A dental assessment of biological affinity between inhabitants of the Gebel Ramlah and R12 Neolithic sites. In Z. Sulgostowska & A. J. Tomaszewski (Eds.), *Man - millennia - environment: Studies in honour of professor Romuald Schild* (pp. 45–52). Institute of Archaeology and Ethnology, Polish Academy of Sciences.

Irish, J. D. (2010). The mean measure of divergence: Its utility in model-free and model-bound analyses relative to the Mahalanobis D^2 distance for nonmetric traits. *American Journal of Human Biology*, 22(3), 378–395.

Irish, J. D., Bailey, S. E., Guatelli-Steinberg, D., Delezene, L. K., & Berger, L. R. (2018). Ancient teeth, phenetic affinities, and African hominins: Another look at where *Homo naledi* fits in. *Journal of Human Evolution*, 122, 108–123.

Irish, J. D., Guatelli-Steinberg, D., Legge, S. S., de Ruiter, D. J., & Berger, L. R. (2013). Dental morphology and the phylogenetic "place" of *Australopithecus sediba*. *Science*, 340(6129), 1233062-1–1233062-4.

Irish, J. D., Guatelli-Steinberg, D., Legge, S. S., de Ruiter, D. J., & Berger, L. R. (2014). Response to 'non-metric dental traits and hominin phylogeny' by Carter et al., with additional information on the Arizona State University dental anthropology system and phylogenetic 'place' of *Australopithecus sediba*. *Journal of Human Evolution*, 69, 9–14.

Irish, J. D., & Hemphill, B. E. (2001). Les Canaries ont-elles été colonisées par les Berbères d'Afrique du Nord? La contribution de l'analyse odontométrique. In D. Hadjouis & B. Mafart (Eds.), *La paléo-odontologie: Analyses et méthodes d'etude collection paléoanthropologie et paléopathologie osseuse* (pp. 122–137). Editions Artcom.

Irish, J. D., Hemphill, B. E., de Ruiter, D. J., & Berger, L. R. (2016). The apportionment of tooth size and its implications in *Australopithecus sediba* versus other Plio-pleistocene and recent African hominins. *American Journal of Physical Anthropology*, 161(3), 398–413.

Irish, J. D., & Kenyhercz, M. (2013). Size does matter: Variation in tooth size apportionment among major regional north and sub-Saharan African populations. *Dental Anthropology*, 26, 38–44.

Jacob, T. (1973). Palaeoanthropological discoveries in Indonesia with special reference to the finds of the last two decades. *Journal of Human Evolution*, 2, 473–485.

Jones, A. S., & Butler, R. J. (2018). A new phylogenetic analysis of Phytosauria (Archosauria: Pseudosuchia) with the application of continuous and geometric morphometric character coding. *PeerJ*, 6, e5901.

Joordens, J. C., Dupont-Nivet, G., Feibel, C. S., Spoor, F., Sier, M. J., van der Lubbe, J. H., Nielsen, T. K., Knul, M. V., Davies, G. R., & Vonhof, H. B. (2013). Improved age control on early *Homo* fossils from the upper Burgi member at Koobi Fora, Kenya. *Journal of Human Evolution*, 65, 731–745.

Jungers, W. L., Falsetti, A. B., & Wall, C. E. (1995). Shape, relative size, and size-adjustments in morphometrics. *American Journal of Physical Anthropology*, 38(S21), 137–161.

Kaifu, Y., Aziz, F., & Baba, H. (2005). Hominid mandibular remains from Sangiran: 1952–1986 collection. *American Journal of Physical Anthropology*, 128(3), 497–519.

Kass, R. E., & Raftery, A. E. (1993) *Bayes factors and model uncertainty. Technical report No. 254*. Seattle: University of Washington.

Kass, R. E., & Raftery, A. E. (1995). Bayes factors. *Journal of the American Statistical Association*, 90(430), 773–795.

Kato, A., & Ohno, N. (2009). Construction of three-dimensional tooth model by micro-computed tomography and application for data sharing. *Clinical Oral Investigations*, 13(1), 43–46.

Kavanagh, K. D., Evans, A. R., & Jernvall, J. (2007). Predicting evolutionary patterns of mammalian teeth from development. *Nature*, 449(7161), 427–432.

Kay, R. F. (2015). Biogeography in deep time–what do phylogenetics, geology, and paleoclimate tell us about early platyrrhine evolution? *Molecular Phylogenetics and Evolution*, 82, 358–374.

Kenyhercz, M. W., & Passalacqua, N. V. (2016). Missing data imputation methods and their performance with biodistance analyses. In M. A. Pillhoud & J. T. Hefner (Eds.), *Biological distance analysis: Forensic and bioarchaeological perspectives* (pp. 181–194). Elsevier.

Kieser, J. A. (1990). *Human adult odontometrics*. Cambridge University Press.

Kivell, T. L., Deane, A. S., Tocheri, M. W., Orr, C. M., Schmid, P., Hawks, J., Berger, L. R., & Churchill, S. E. (2015). The hand of *Homo naledi*. *Nature Communications*, 6(1), 1–9.

Klingenberg, C. P. (2014). Studying morphological integration and modularity at multiple levels: Concepts and analysis. *Philosophical Transactions of the Royal Society B: Biological Sciences*, 369(1649), 20130249.

Kluge, A. G. (1989). A concern for evidence and a phylogenetic hypothesis of relationships among epicrates (*Boidae, Serpentes*). *Systematic Biology*, 38, 7–25.

Kruskal, J. B., & Wish, M. (1978). *Multidimensional scaling*. Sage Publications.

Kuhner, M. K., & Felsenstein, J. (1994). A simulation comparison of phylogeny algorithms under equal and unequal evolutionary rates. *Molecular Biology and Evolution*, 11(3), 459–468.

Kupczik, K., Delezene, L. K., & Skinner, M. M. (2019). Mandibular molar root and pulp cavity morphology in *Homo naledi* and other Plio-Pleistocene hominins. *Journal of Human Evolution*, 130, 83–95.

Lajeunesse, M. J., & Fox, G. A. (2015). Statistical approaches to the problem of phylogenetically correlated data. In G. J. Fox, S. Negrete-Yankelevitch, & V. J. Sosa (Eds.), *Ecological statistics: Contemporary theory and application* (pp. 261–283). Oxford University Press.

Langergraber, K. E., Prüfer, K., Rowney, C., Boesch, C., Crockford, C., Fawcett, K., Inoue, E., Inoue-Muruyama, M., Mitani, J. C., Muller, M. N., & Robbins, M. M. (2012). Generation times in wild chimpanzees and gorillas suggest earlier divergence times in great ape and human evolution. *Proceedings of the National Academy of Sciences*, 109, 15716–15721.

Lee, M. S., Cau, A., Naish, D., & Dyke, G. J. (2014). Morphological clocks in paleontology, and a mid-cretaceous origin of crown Aves. *Systematic Biology*, 63, 442–449.

Lewis, P. O. (2001). A likelihood approach to estimating phylogeny from discrete morphological character data. *Systematic Biology*, 50, 913–925.

Lordkipanidze, D., de León, M. S. P., Margvelashvili, A., Rak, Y., Rightmire, G. P., Vekua, A., & Zollikofer, C. P. (2013). A complete skull from Dmanisi, Georgia, and the Evolutionary Biology of Early *Homo*. *Science*, 342, 326–331.

Lukacs, J. R., & Hemphill, B. E. (1993). Odontometry and biological affinity in South Asia: Analysis of three ethnic groups from Northwest India. *Human Biology*, 65, 279–325.

Lycett, S. J., & Collard, M. (2005). Do homoiologies impede phylogenetic analyses of the fossil hominids? An assessment based on extant

papionin craniodental morphology. *Journal of Human Evolution*, 49(5), 618–642.

Maddison, W. (1989). Reconstructing character evolution on polytomous cladograms. *Cladistics*, 5(4), 365–377.

Maddison, W. P. (2000). Testing character correlation using pairwise comparisons on a phylogeny. *Journal of Theoretical Biology*, 202(3), 195–204.

Mahler, P. E. (1973). *Metric variation in the pongid dentition* [PhD Dissertation, University of Michigan, Ann Arbor]. ProQuest Dissertations Publishing.

Marchi, D., Walker, C. S., Wei, P., Holliday, T. W., Churchill, S. E., Berger, L. R., & DeSilva, J. M. (2017). The thigh and leg of *Homo naledi*. *Journal of Human Evolution*, 104, 174–204.

Martinón-Torres, M., de Castro, J. M. B., Gómez-Robles, A., Margvelashvili, A., Prado, L., Lordkipanidze, D., & Vekua, A. (2008). Dental remains from Dmanisi (Republic of Georgia): Morphological analysis and comparative study. *Journal of Human Evolution*, 55(2), 249–273.

Martins, E. P., & Hansen, T. F. (1997). Phylogenies and the comparative method: A general approach to incorporating phylogenetic information into the analysis of interspecific data. *The American Naturalist*, 149(4), 646–667.

Mitteroecker, P., & Gunz, P. (2009). Advances in geometric morphometrics. *Evolutionary Biology*, 36(2), 235–247.

Mongle, C. S., Strait, D. S., & Grine, F. E. (2019). Expanded character sampling underscores phylogenetic stability of *Ardipithecus ramidus* as a basal hominin. *Journal of Human Evolution*, 131, 28–39.

Moorrees, C. F. A., & Reed, R. B. (1964). Correlations among crown diameters of human teeth. *Archives of Oral Biology*, 9, 685–697.

Nascimento, F. F., Dos Reis, M., & Yang, Z. (2017). A biologist's guide to Bayesian phylogenetic analysis. *Nature Ecology & Evolution*, 1(10), 1446–1454.

Nixon, K. C., & Wheeler, Q. D. (1992). Extinction and the origin of species. In M. J. Novacek & Q. D. Wheeler (Eds.), *Extinction and phylogeny* (pp. 119–143). Columbia University Press.

O'Leary, M. A., Bloch, J. I., Flynn, J. J., Gaudin, T. J., Giallombardo, A., Giannini, N. P., Goldberg, S. L., Kraatz, B. P., Luo, Z. X., Meng, J., & Ni, X. (2013). The placental mammal ancestor and the post–K-Pg radiation of placentals. *Science*, 339(6120), 662–667.

O'Leary, M. A., & Geisler, J. H. (1999). The position of Cetacea within Mammalia: Phylogenetic analysis of morphological data from extinct and extant taxa. *Systematic Biology*, 48(3), 455–490.

Parins-Fukuchi, C. (2018a). Use of continuous traits can improve morphological phylogenetics. *Systematic Biology*, 67(2), 328–339.

Parins-Fukuchi, C. (2018b). Bayesian placement of fossils on phylogenies using quantitative morphometric data. *Evolution*, 72(9), 1801–1814.

Penrose, L. S. (1954). Distance, size and shape. *Annals of Eugenics*, 18, 337–343.

Pimentel, R. A., & Riggins, R. (1987). The nature of cladistic data. *Cladistics*, 3(3), 201–209.

Poe, S., & Wiens, J. J. (2000). Character selection and the methodology of morphological phylogenetics. In J. J. Wiens (Ed.), *Phylogenetic analysis of morphological data* (pp. 20–36). Smithsonian Institution Press.

Pogue, M. G., & Mickevich, M. F. (1990). Character definitions and character state delineation: The bête noire of phylogenetic inference. *Cladistics*, 6(4), 319–361.

Pol, D., & Escapa, I. H. (2009). Unstable taxa in cladistic analysis: Identification and the assessment of relevant characters. *Cladistics*, 25(5), 515–527.

Polly, P. D., Lawing, A. M., Fabre, A. C., & Goswami, A. (2013). Phylogenetic principal components analysis and geometric morphometrics. *Hystrix, the Italian Journal of Mammalogy*, 24(1), 33–41.

Polly, P.D. (2007). Development with a bite. *Nature*, 449(7161), 413–414.

Purvis, A., & Garland, T. (1993). Polytomies in comparative analyses of continuous characters. *Systematic Biology*, 42(4), 569–575.

Pybus, O. G. (2006). Model selection and the molecular clock. *PLoS Biol*, 4(5), e151.

Rahman, N. A. (1962). On the sampling distribution of the studentized Penrose measure of distance. *Annals of Human Genetics*, 26(2), 97–106.

Richter, D., Grün, R., Joannes-Boyau, R., Steele, T. E., Amani, F., Rué, M., Fernandes, P., Raynal, J. P., Geraads, D., Ben-Ncer, A., & Hublin, J. J. (2017). The age of the hominin fossils from Jebel Irhoud, Morocco, and the origins of the Middle Stone Age. *Nature*, 546(7657), 293–296.

Rightmire, G. P., & Lordkipanidze, D. (2010). The first hominin colonization of Eurasia. In J. G. Fleagle, J. J. Shea, F. E. Grine, A. L. Baden, & R. E. Leakey (Eds.), *Out of Africa I: The first hominin colonization of Eurasia* (pp. 225–243). Springer.

Rizk, O. T., Amugongo, S. K., Mahaney, M. C., & Hlusko, L. J. (2008). The quantitative genetic analysis of primate dental variation: History of the approach and prospects for the future. In J. D. Irish & G. C. Nelson (Eds.), *Technique and application in dental anthropology* (pp. 317–346). Cambridge University Press.

Ronquist, F., & Huelsenbeck, J. P. (2003). MrBayes 3: Bayesian phylogenetic inference under mixed models. *Bioinformatics*, 19(12), 1572–1574.

Ronquist, F., Huelsenbeck, J.P., Teslenko, M., & Nylander, J.A.A. (2020). MrBayes version 3.2 manual: Tutorials and model summaries. https://nbisweden.github.io/MrBayes/manual.html

Schols, P., D'hondt, C., Geuten, K., Merckx, V., Janssens, S., & Smets, E. (2004). MorphoCode: Coding quantitative data for phylogenetic analysis. *PhyloInformatics*, 4, 1–4.

Schroer, K., & Wood, B. (2015). Modeling the dental development of fossil hominins through the inhibitory cascade. *Journal of Anatomy*, 226(2), 150–162.

Schroeder, L., Scott, J. E., Garvin, H. M., Laird, M. F., Dembo, M., Radovčić, D., Berger, L. R., de Ruiter, D. J., & Ackermann, R. R. (2017). Skull diversity in the *Homo* lineage and the relative position of *Homo naledi*. *Journal of Human Evolution*, 104, 124–135.

Scotland, R. W., Olmstead, R. G., & Bennett, J. R. (2003). Phylogeny reconstruction: The role of morphology. *Systematic Biology*, 52(4), 539–548.

Smith, H. F., & Grine, F. E. (2008). Cladistic analysis of early *Homo* crania from Swartkrans and Sterkfontein, South Africa. *Journal of Human Evolution*, 54(5), 684–704.

Sokal, R. R., & Sneath, P. H. A. (1963). *Principles of numerical taxonomy*. WH Freeman.

Spoor, F., Gunz, P., Neubauer, S., Stelzer, S., Scott, N., Kwekason, A., & Dean, M. C. (2015). Reconstructed *Homo* habilis type OH 7 suggests deep-rooted species diversity in early Homo. *Nature*, 519(7541), 83–86.

Stadler, T. (2010). Sampling-through-time in birth–death trees. *Journal of Theoretical Biology*, 267(3), 396–404.

Stadler, T., Gavryushkina, A., Warnock, R. C., Drummond, A. J., & Heath, T. A. (2018). The fossilized birth-death model for the analysis of stratigraphic range data under different speciation modes. *Journal of Theoretical Biology*, 447, 41–55.

Steiper, M. E., & Seiffert, E. R. (2012). Evidence for a convergent slowdown in primate molecular rates and its implications for the timing of early primate evolution. *Proceedings of the National Academy of Sciences*, 109(16), 6006–6011.

Stevens, P. F. (1991). Character states, morphological variation, and phylogenetic analysis: A review. *Systematic Botany*, 16, 553–583.

Stojanowski, C. M., Paul, K. S., Seidel, A. C., Duncan, W. N., & Guatelli-Steinberg, D. (2017). Heritability and genetic integration of tooth size in the South Carolina Gullah. *American Journal of Physical Anthropology*, 164(3), 505–521.

Strait, D. S., & Grine, F. E. (2004). Inferring hominoid and early hominid phylogeny using craniodental characters: The role of fossil taxa. *Journal of Human Evolution*, 47(6), 399–452.

Strait, D. S., Grine, F. E., & Moniz, M. A. (1997). A reappraisal of early hominid phylogeny. *Journal of Human Evolution*, *32*(1), 17–82.

Thackeray, F. (2015). Estimating the age and affinities of *Homo naledi*. *South African Journal of Science*, *111*(11–12), 1–2.

Thiele, K. (1993). The holy grail of the perfect character: The cladistic treatment of morphometric data. *Cladistics*, *9*(3), 275–304.

Townsend, G., Harris, E. F., Lesot, H., Clauss, F., & Brook, A. (2009). Morphogenetic fields within the human dentition: A new, clinically relevant synthesis of an old concept. *Archives of Oral Biology*, *54*, S34–S44.

Townsend, G., Richards, L., & Hughes, T. (2003). Molar intercuspal dimensions: Genetic input to phenotypic variation. *Journal of Dental Research*, *82*(5), 350–355.

Townsend, G. C., & Brown, T. (1980). Dental asymmetry in Australian aboriginals. *Human Biology*, *52*, 661–673.

VanSickle, C., Cofran, Z., García-Martínez, D., Williams, S. A., Churchill, S. E., Berger, L. R., & Hawks, J. (2018). *Homo naledi* pelvic remains from the Dinaledi chamber, South Africa. *Journal of Human Evolution*, *125*, 122–136.

Veneziano, A., Irish, J. D., Meloro, C., Stringer, C., & De Groote, I. (2019). The functional significance of dental and mandibular reduction in *Homo*: A catarrhine perspective. *American Journal of Primatology*, *81*(3), e22953.

von Cramon-Taubadel, N. (2009). Revisiting the homoiology hypothesis: The impact of phenotypic plasticity on the reconstruction of human population history from craniometric data. *Journal of Human Evolution*, *57*(2), 179–190.

Weidenreich, F. (1937). The dentition of Sinanthropus pekinensis. A comparative odontography of the hominids. *Paleontlogica Sinica*, *101*(1), 1–180.

Weidenreich, F. (1945). Giant early man from Java and South China. *Anthropological Papers of the American Museum of Natural History*, *40*, 1–134.

White, T. D., WoldeGabriel, G., Asfaw, B., Ambrose, S., Beyene, Y., Bernor, R. L., Boisserie, J. R., Currie, B., Gilbert, H., Haile-Selassie, Y., Hart, W. K., & Suwa, G. (2006). Asa Issie, Aramis and the origin of *Australopithecus*. *Nature*, *440*(7086), 883–889.

Wiens, J. J. (1995). Polymorphic characters in phylogenetic systematics. *Systematic Biology*, *44*(4), 482–500.

Wiens, J. J. (2001). Character analysis in morphological phylogenetics: Problems and solutions. *Systematic Biology*, *50*(5), 689–699.

Wiens, J. J. (2004). The role of morphological data in phylogeny reconstruction. *Systematic Biology*, *53*(4), 653–661.

Wiens, J. J., & Hillis, D. M. (1996). Accuracy of parsimony analysis using morphological data: A reappraisal. *Systematic Botany*, *21*, 237–234.

Williams, S., García-Martínez, D., Bastir, M., Meyer, M. R., Nalla, S., Hawks, J., Schid, P., Churchill, S. E., & Berger, L. R. (2016). The vertebrae and ribs of *Homo naledi*. *Journal of Human Evolution*, *30*(1), e19.

Wood, B., & Collard, M. (1999). The human genus. *Science*, *284*(5411), 65–71.

Wood, B., & Lonergan, N. (2008). The hominin fossil record: Taxa, grades and clades. *Journal of Anatomy*, *212*(4), 354–376.

Wood, B. A. (1991). *Koobi Fora research project: Volume 4, hominid crania remains*. Clarendon Press.

Wood, B. A., & Patterson, D. B. (2020). *Paranthropus* through the looking glass. *Proceedings of the National Academy of Sciences*, *117*(38), 23202–23204.

Wright, A. M., & Hillis, D. M. (2014). Bayesian analysis using a simple likelihood model outperforms parsimony for estimation of phylogeny from discrete morphological data. *PLoS One*, *9*(10), e109210.

Wu, J.-K., & Chia, L. P. (1954). New discoveries about Sinanthropus pekinensis in Choukoutien. *Acta Palaeontologica Sinica*, *2*, 267–288.

Wu, X., & Poirier, F. E. (1995). *Human evolution in China: A metric description of the fossils and a review of the sites*. Oxford University Press.

Xie, W., Lewis, P. O., Fan, Y., Kuo, L., & Chen, M. H. (2011). Improving marginal likelihood estimation for Bayesian phylogenetic model selection. *Systematic Biology*, *60*(2), 150–160.

Xing, S., Martinón-Torres, M., & de Castro, J. M. B. (2018). The fossil teeth of the Peking man. *Scientific Reports*, *8*(1), 1–11.

Zaim, Y., Ciochon, R. L., Polanski, J. M., Grine, F. E., Bettis, E. A., III, Rizal, Y., Franciscus, R. G., Larick, R. R., Heizler, M., Eaves, K. L., & Marsh, H. E. (2011). New 1.5 million-year-old *Homo erectus* maxilla from Sangiran (Central Java, Indonesia). *Journal of Human Evolution*, *61*(4), 363–376.

Zhang, C., Stadler, T., Klopfstein, S., Heath, T. A., & Ronquist, F. (2016). Total-evidence dating under the fossilized birth–death process. *Systematic Biology*, *65*(2), 228–249.

SUPPORTING INFORMATION

Additional supporting information may be found online in the Supporting Information section at the end of this article.